

We are IntechOpen, the world's leading publisher of Open Access books Built by scientists, for scientists

6,900

Open access books available

186,000

International authors and editors

200M

Downloads

Our authors are among the

154

Countries delivered to

TOP 1%

most cited scientists

12.2%

Contributors from top 500 universities



WEB OF SCIENCE™

Selection of our books indexed in the Book Citation Index
in Web of Science™ Core Collection (BKCI)

Interested in publishing with us?
Contact book.department@intechopen.com

Numbers displayed above are based on latest data collected.
For more information visit www.intechopen.com



Unravelling Glycobiology by NMR Spectroscopy

Vitor H. Pomin

Additional information is available at the end of the chapter

<http://dx.doi.org/10.5772/48136>

1. Introduction

1.1. NMR spectroscopy: Approaching glycobiology

Generally speaking, nuclear magnetic resonance (NMR) spectroscopy seems the most powerful technique in current use for structural analysis of biomolecules. Four Nobel prizes have been awarded so far due to discoveries related to NMR: 1952 (Physics) to Felix Bloch and Edward Mills Purcell for explanations of the physical properties of nuclei under magnetization; 1991 (Chemistry) to Richard Ernest for the development of the principles for the multidimensionality in NMR spectroscopy; 2002 (Chemistry) to Kurt Wüthrich for applying NMR in structural determination of biomolecules, mainly proteins; and 2003 (Medicine) for Paul Lauterbur and Peter Mansfield to the discoveries concerning the use of magnetic resonance imaging in medical diagnostics. The significant boom of NMR spectroscopy in structural biology however dates from the beginning of 80's, mainly due to the implementation of two-dimensional techniques associated with advances in instrumentation and *in vivo* or *in vitro* methods for making suitable samples for NMR analysis (especially labeling procedures of NMR-active nuclei) [1].

Particularly, we could generalize that in the following two decades, proteins and nucleic acids were the primary biomolecule types in NMR studies. This was somewhat related to the usual 3D structures these molecules may present in solution. This consequently facilitates the detection of valuable spatial contacts between residues that are displaced away in a polymeric chain. The achievements by NMR in studies of proteins and nucleic acids were also significant to push the genome and proteome projects. Although, carbohydrates were also analyzed by NMR at this period, the association between glycobiology and NMR was somewhat neglected. For sure, this has happened because of the general idea of high structural complexity of carbohydrates combined with their high-order dynamic properties (high molecular flexibility). The conception of an unclear or absent three-dimensional states for carbohydrate molecules was one of the greatest reasons to this limited attention.

However, persistent research groups worldwide have been proving otherwise and showed to the community interesting NMR results concerning glycans. These results have helped to unravel the biological roles of glycans. Above all, since that time, glycobiology turned to be a fertile field for NMR spectroscopy. Due to the current glycomics' boom, the high number of vital biological roles triggered by carbohydrate molecules, and the advances in NMR methods, NMR and glycobiology are now a very promising combination. Hence, in this chapter, we want to illustrate this new trend. For this, we cover the basis of the major solution NMR methods in glycobiology, taking examples from our experiments or from published works. We offer to the readership the adequate conclusions of these NMR data and moreover, what they represent for explaining the physicochemical mechanisms of the glycans addressed.

2. The essential high-throughput NMR methods exploited in glycobiology

NMR spectroscopy has a special position compared to the other analytical techniques once it provides a variety of experiment types to be performed as many as structural features to investigate in a biologically relevant macromolecule. Moreover, the NMR studies can be performed in solution which can mimic the physiological conditions. The major disadvantages in application of NMR spectroscopy are that of sensitivity and limitation in high-molecular mass systems. In order to overcome respectively these two obstacles, methods of *in vitro* or *in vivo* isotopic labeling with specific magnetically active nuclear spins (principally ^{13}C and ^{15}N) [2,3] and new pulse sequences to specifically reduce losses from transverse relaxation mechanisms [4-6] were developed along the years. These methods, established primarily to proteins and nucleic acids [4-9], are now being used to study carbohydrates and glycoconjugates as well [10,11].

Among many NMR techniques to be applied in glycobiology, we shall explain the most basic and utilized ones, such as 1) information from different NMR-active isotopes (^1H , ^{13}C , ^{15}N); 2) cross-peak assignments through multi-dimensional NMR spectra for tabulating chemical shift values or structural characterization purposes; 3) dynamic studies by measurements of longitudinal or spin-lattice (T_1) and transversal or spin-spin (T_2) relaxation rates (R_1 and R_2 , respectively, in ms to s), and of line-widths or line broadening (in Hz) in certain NMR timescale; 4) chemical shift changes (in ppm) that may reflect conformational changes in carbohydrates due to temperature variations, or in carbohydrate-binding proteins in the presence of ligands where localized chemical shift perturbation is induced by presence of intermolecular contacts; 5) measurements of constants of either scalar (J) or dipolar (D) couplings (in Hz) and their contribution to the averaged conformational shape of carbohydrates or oligosaccharides, and 6) NOE-based through space contacts for determination of sugar preferential conformational shapes in solution or in studies of intermolecular complexes, especially those of carbohydrate-protein interactions. The NMR data presented herein is discussed with the primary objective to help the readership in NMR data interpretation and thus conclusions about the physicochemical properties of certain glycans in solution.

2.1. The NMR-active isotopes mostly used in carbohydrate studies

The three isotopes with magnetically active nuclei spin- $\frac{1}{2}$ mostly studied in glycobiology NMR are ^1H , ^{13}C , and ^{15}N . Each one has its own magnetic relative susceptibility (Table 1), its own precessional frequency (Larmor frequencies at 800 MHz for ^1H , for example, in Table 1), relaxation properties, and principally differential atomic positions within a molecule. These differenced localizations ultimately provide useful information concerning structural features, in the atomic perspective, and dynamic properties, of specific regions or sites within a molecule. In dynamic studies, localized motions as well as global motions of the analyzed molecules can also be evaluated, depending on the atom or group of atoms that have to be examined. It is worth mentioning that the relative NMR receptivity (dependent on the isotopomeric abundance, relaxation and magnetogyric ratio) of these three biomolecularly abundant NMR-active isotopes is quite different, which leads to different NMR sensitivity. While ^1H has its value set as 1.0, ^{13}C and ^{15}N have their values as 1.76×10^{-4} , and 3.85×10^{-6} (Table 1).

Nuclide	Spin	Natural abundance	Gyromagnetic ratio γ [$10^7 \text{ rad T}^{-1} \text{ s}^{-1}$]	NMR Frequency (at 18.8 Tesla)	Relative receptivity
Proton (^1H)	$\frac{1}{2}$	99.985	26.7522	799.734 (1)	1.00
Carbon-12 (^{12}C)	0	98.9	-	-	-
Carbon-13 (^{13}C)	$\frac{1}{2}$	1.108	6.7283	201.133 (1/3.976)	6.73×10^{-7}
Nitrogen-14 (^{14}N)	1	99.63	1.9338	57.820 (1/13.831)	1.00×10^{-3}
Nitrogen-15 (^{15}N)	$\frac{1}{2}$	0.37	-2.7126	81.093 (1/9.861)	3.85×10^{-6}

Table 1. Some nuclei properties important for NMR detection.

In principle, one would say it would be one of the greatest luck for NMR spectroscopists, the existence of biomolecules, including carbohydrates, rich in sensitive and active isotopes for NMR studies (Table 1). This is true if we consider the essential magnetic properties and abundance of hydrogen atoms in such molecules. Coincidentally or not, in proteins, nucleic acids, lipids, and not differently in carbohydrates, hydrogen is not the most abundant atom, but it also fundamentally participates directly (by physical contacts) in many of the biological reactions, either through hydrogen-bond networks in protonated states during binding events, or even indirectly because of its absence in deprotonated states during pH-changes occurred during physiological reactions. Therefore, one would guess that ^1H -atoms would be the most used isotope in NMR analysis, and this is exactly what happens not only for glycomics but also for lipidomics, proteomics, and genomics. The changes and profiles of

^1H -signal distribution are informative in terms of molecular states, reactions, and dynamics, as exemplified by the simple mutarotation changes of the anomeric hydrogens of reducing terminal sugars in solution as a function of time (Figure 1). For example, only a simple structural change at the C2 of the glucose (Glc)-derived monosaccharides is enough to cause kinetic alterations of the ^1H -anomerics equilibrium in solution. The intensities of the ^1H -peaks properly indicate the proportion of these protons within a molecule, and therefore they are extremely useful to estimate the atoms and the percentage of each enantiomeric form (percentages in Figure 1). Actually, just after mass spectrometry (MS) techniques, measurements based on integrals of ^1H -signals seem to be the most reliable quantitative procedure to determine the number of atoms within a molecule, as well as their conformational states.

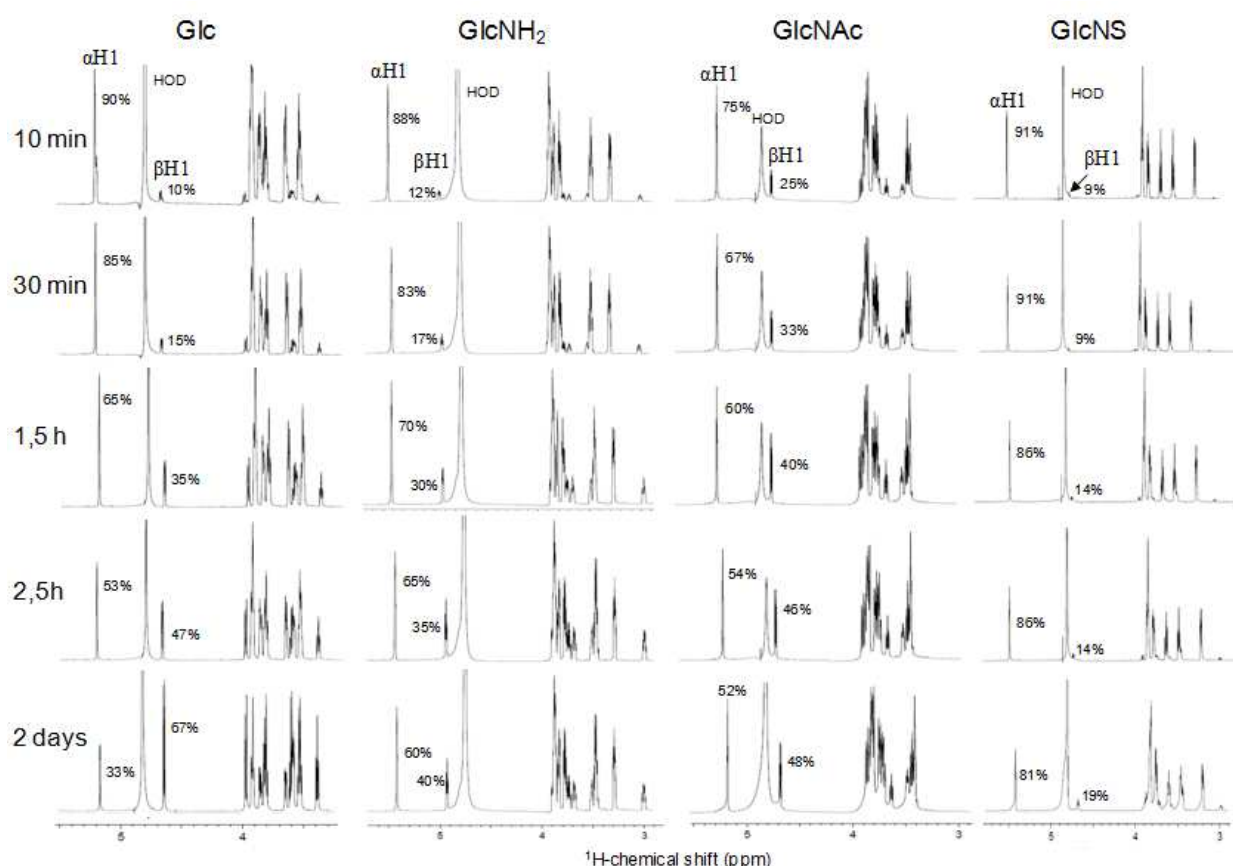


Figure 1. 1D ^1H -NMR spectra of glucose (Glc), and its derivatives: glucosamine (GlcNH₂), *N*-acetylglucosamine (GlcNAc), and *N*-sulfated glucosamine (GlcNS), all in $\sim 100\%$ D₂O-solution. The spectra were recorded in a Varian 800 MHz spectrometer at 25°C and at different time courses after dissolution, as indicated in the left of the panel. The percentage of the α - and β - ^1H -anomerics changes as a function of time at different rates accordingly to the monosaccharide type, solvent and temperature. The water (HOD) and anomeric signals are indicated at the top of the panel.

The profile of ^1H -signals in 1D ^1H -NMR spectra offers a general fingerprint of the biomolecule in a solution such as the degree of pureness crucial for carbohydrates with biomedical purposes. However, due to the large density of protons in biomolecules,

including carbohydrates, sometimes the ^1H -NMR profile is overwhelming because of the many condensed, overlapped and thus unresolved signals. Therefore, the use of other nuclei such as ^{13}C and ^{15}N , either coupled or uncoupled to ^1H , becomes valuable and complementary in the analyses, resulting important conclusions with respect the physicochemical properties of carbohydrates. For example, the intensity of ^{13}C -signals of anomeric can also be diagnostic for the changing rates of the α - and β -states during mutarotation in solution, as demonstrated below. The directly observed ^{13}C -signals are frequently much sharper than ^1H -signals due to its differential relaxation property. The thinner ^{13}C -signals in 1D NMR profile result usually more well-resolved peaks, and through the unidimensional scale, less superimpositions should occur. This is exactly what happens in structural analyses of algal sulfated polysaccharides with high degrees of structural heterogeneities [12-14]. ^1H -coupled ^{13}C -signals are very diagnostic of the methine (CH), methylene (CH_2) and methyl (CH_3) groups highly abundant in carbohydrate molecules, and thus quite useful in NMR structural glycobiology. In case of carbohydrates or glycosylated molecules that contain amino sugars, like the glycosaminoglycans (GAGs) that bear hexosamines with ^{15}N -natural abundant amino groups, the ^{15}N -related NMR signals although few in number are well-resolved and still quite useful for structural diagnosis [10]. Hence, hetero-atoms are very useful in solution NMR structural glycobiology through multi-dimensional heteronuclear experiments, or in direct observe experiments, as discussed next to describe the assignments of glucose and the novel method for characterizing GAG molecules through ^{15}N -atoms.

2.2. Peak assignments through multi-dimensional NMR spectra of glycans

Although ^1H -NMR spectra are quite informative in terms of the general view of the molecule and diagnostic for the presence of contamination, fully protonated molecules with high-molecular weights, and with a certain degree of heterogeneity, result in very complex ^1H -NMR spectra. This can be seen by the presence of many unresolved peaks from polysaccharides with no clear pattern of structural regularity. In general, in glycan analysis, except the ^1H -signals belonging to the anomeric that resonate at the most downfield region of the spectra (usually located somewhere between 4.5 and 6.0 ppm), all other ring protons from the most monosaccharide types resonate very squeezedly between 3.0 and 4.5 ppm. This can be seen through the 1D ^1H -NMR spectrum in solution of the simple and most common monosaccharide, the glucopyranose (Glc_p) (Figure 2B) after reaching the anomeric equilibrium in solution (Figure 1). The low chemical shift dispersion (also called chemical shift degeneracy) typical of carbohydrates makes assignments of individual peaks hard of full accomplishment, and thus the acquisition of 2D homonuclear NMR spectra becomes essential for further structural ^1H -assignments. The combination of some 2D homonuclear ^1H -based spectra together with the 1D ^1H -NMR facilitates resonance assignments as exemplified with the acquisition and annotation of the correlation spectroscopy (COSY) and total correlation spectroscopy (TOCSY) spectra of glucose (Figure 3). This procedure allows the proper full assignment of all chemical shifts that belong to non-exchangeable protons (in black in structures of Figure 2A).

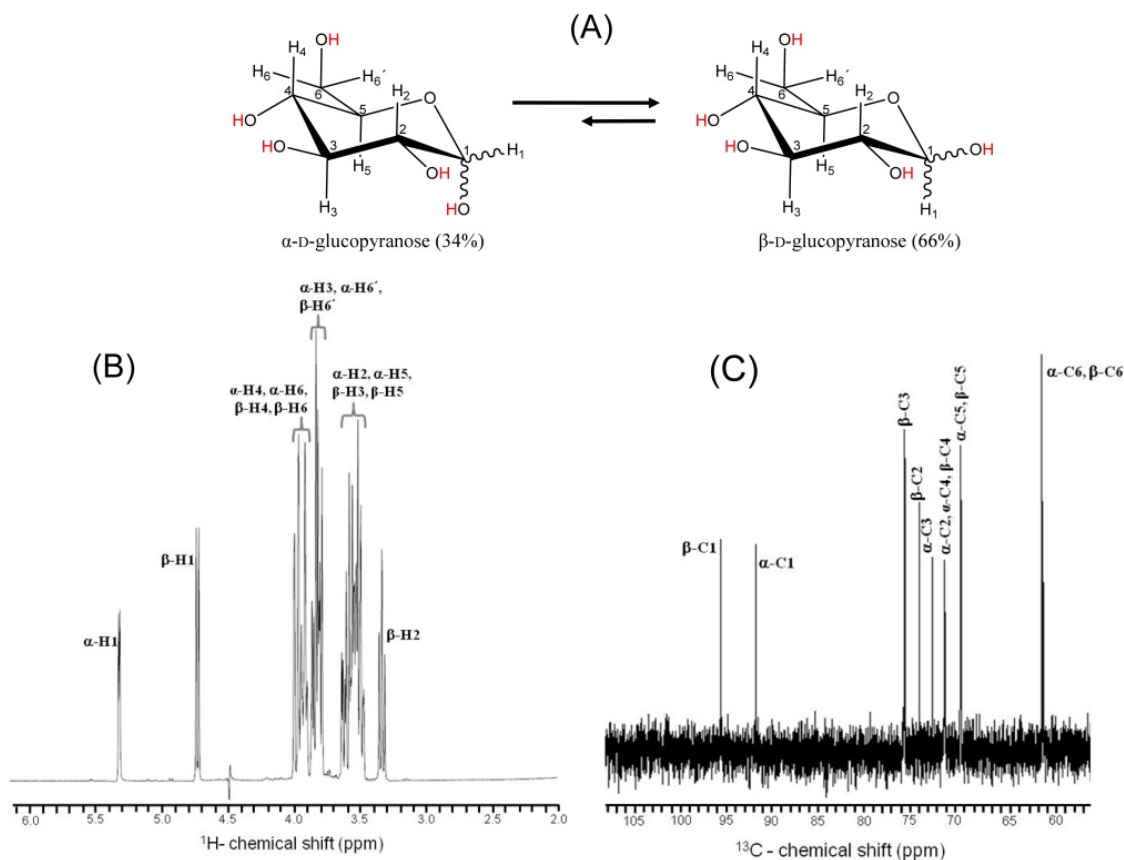


Figure 2. (A) Structural representation of D-glucose and its anomeric configurations (α - and β -forms) in aqueous solution. The numbers of the hydrogen and carbon atoms are indicated by digits, and the solvent exchangeable protons are red-colored. (B) ^1H - and (C) ^{13}C -NMR 1D spectra, Bruker 400 MHz and 37°C of D-glucose in solution after waiting to reach the anomeric equilibrium (2 days as shown at Figure 1). The signals are labeled according to the atom numbers and anomeric forms designated in the molecules represented on panel A.

Observing either the 1D ^1H -NMR spectrum (Figure 2B), or the 2D ^1H -based NMR spectra (Figure 3A, and 3B), it is clear that the anomeric ^1H -signals at the downfield region of the suppressed water (HOD) peak at ~ 4.50 ppm are well-resolved, and thus they may serve as good starting-points to trace connectivities using 2D-NMR spectra. Usually, α - ^1H -anomeric signals resonate more downfield than β -ones in the majority of the carbohydrate units. In the case of glucose, the α - ^1H signals resonate exactly at 5.32 ppm, while the β - ^1H signals resonates exactly at 4.74 ppm (Table 2).

Since COSY experiments create ^1H - ^1H cross-peaks within $^3J_{\text{H}(n)\text{-H}(n+1)}$ (scalar couplings of protons of three-bond distances) like those observed for $^3J_{\text{H}1\text{-H}2}$, $^3J_{\text{H}2\text{-H}3}$, $^3J_{\text{H}3\text{-H}4}$, (Figure 3A), most of the ^1H -chemical shifts (in ppm) for each type of anomeric form of Glc can be assigned (Table 2). The TOCSY spectrum, which gives the full displacement of all J -connected protons (spin systems), can be used either to reinforce the assignments made using COSY or to allow additional assignments which were missing or unclear on the COSY spectrum. Once all ^1H -chemical shifts are properly obtained, the 1D ^1H -NMR spectrum (Figure 2B) can be completely assigned accordingly, and a table of ^1H -chemical shifts can be

filled up. Furthermore, through a carbon-related experiment such as the heteronuclear single quantum coherence (HSQC) spectrum, all ^1H -linked carbons signals can be ultimately assigned through the correlation of the one-bonded ^1H - ^{13}C J -couplings such as $^1J_{\text{H1-C1}}$, $^1J_{\text{H2-C2}}$, $^1J_{\text{H3-C3}}$, and so on. Therefore, all ^{13}C -chemical shifts are finally obtained from previously assigned ^1H -chemical shifts. And the directly observed ^{13}C -NMR spectrum (Figure 2C) can be ultimately assigned as well.

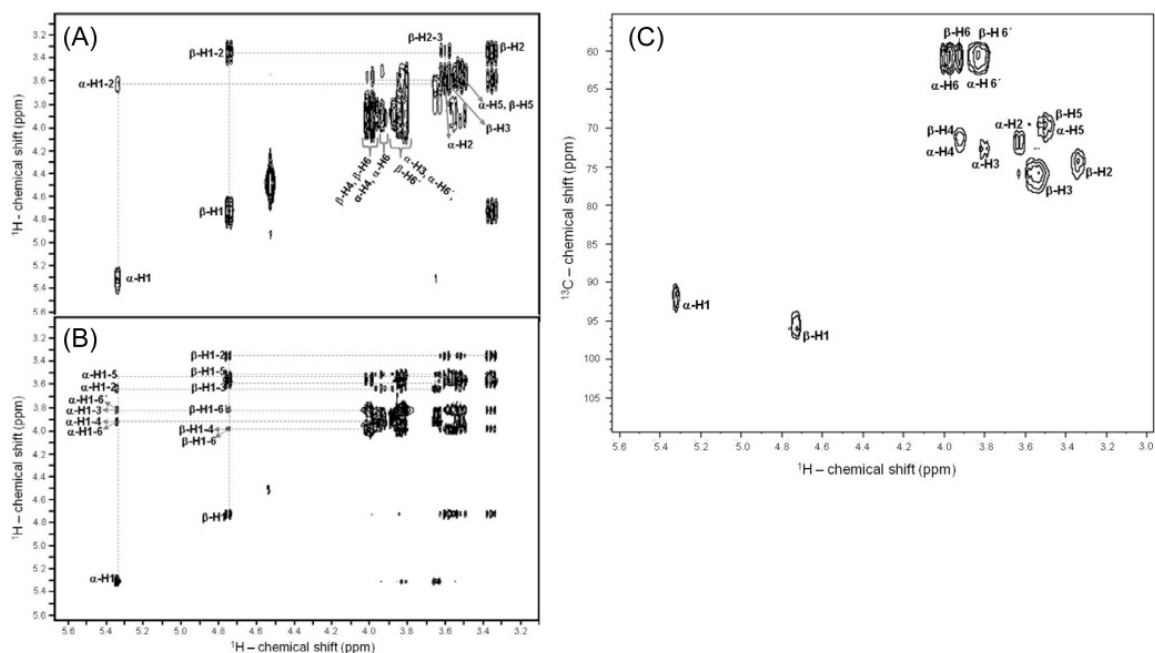


Figure 3. (A) COSY, (B) TOCSY and (C) HSQC spectra, Bruker 400 MHz at 37° C of D-glucose in 100% D_2O -solution after waiting to reach the anomeric equilibrium. The signals are labeled according to the atoms in the molecule (Figure 1A).

α -D-Glcp	β -D-Glcp
α -H1 – 5.32	β -H1 – 4.74
α -H2 – 3.63	β -H2 – 3.37
α -H3 – 3.83	β -H3 – 3.60
α -H4 – 3.92	β -H4 – 3.92
α -H5 – 3.50	β -H5 – 3.5
H6/6' - 3.91/3.82	H6/6' - 3.91/3.82
α -C1 – 91.4	β -C1 – 95.9
α -C2 – 71.8	β -C2 – 74.1
α -C3 – 72.4	β -C3 – 75.8
α -C4 – 71.2	β -C4 – 71.2
α -C5 – 69.8	β -C5 – 69.8
α -C6 – 60.3	β -C6 – 60.3

*Obtained from assignments of NMR spectra at Figures 2B, 2C, and 3.

Table 2. ^1H - and ^{13}C -chemical shifts* of both α - and β -D-Glcp residues.

The downside in collecting spectra containing heteronuclear-filters (either ^{13}C -, or ^{15}N -) even with acquisition through ^1H , such as in the HSQC experiment (Figure 3C) is that it is more time-consuming than those based exclusively on ^1H -atoms. This is because of the sensitivity and abundance of the heteronuclear isotopes, which are much lower than those of proton (see NMR receptivity in Table 1). This can be proved by different signal-to-noise ratio clearly seen by the baseline widths comparatively observed in the 1D ^1H - and ^{13}C -NMR spectra (Figure 2B vs 2C). In ^{13}C -directly observed NMR spectra, the peaks are usually thinner compared to ^1H -signals (Figure 2B vs 2C). This is, in turn, due to different relaxation properties of the ^{13}C -nucleus. The longitudinal or T_1 relaxation of carbons is much faster than protons, which result a considerably sharper peak in 1D NMR (Figure 2B vs 2C).

Due to the lower relative receptivity of heteronucleus, sometimes isotopic labeling techniques are necessary to develop 2D NMR analysis for certain carbohydrates. This is crucial, especially for those cases where the amount of material is a limitation, such as glycans isolated from cell cultures. Recently, we developed an *in vivo* method to spin-label cellular GAG molecules with nitrogen-15 [10] to allow observation and consequently get structural characterization via ^{15}N -chemical shift. This is the third isotope type used in NMR analysis in glycosaminoglycanomics. Our method was based on cell cultures using media enriched in ^{15}N -labeled side-chain glutamine [10]. The side-chain amino group of this amino acid is responsible to donate the NH_2 group to the amino sugar during hexosamine biosynthesis in the cytosol. Through this *in vivo* labeling method, ^{15}N -HSQC spectra became recordable for a couple of few hundred micrograms of GAG isolated from cellular sources [10]. On the other hand, as standard GAGs can be readily available from suppliers, the HSQC spectra using ^{15}N -isotope at natural abundance proved to be successfully recordable at 15 mg/ml concentration-samples within just a couple of hours of acquisition. ^{15}N -HSQC spectrum has been proved to be very straightforward in structural characterization of GAGs in solution (Figure 4).

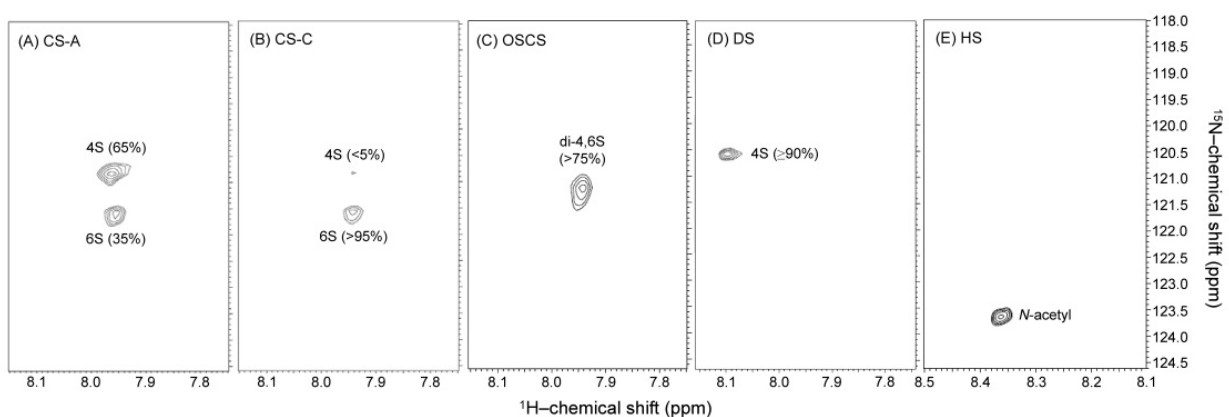


Figure 4. ^{15}N -HSQC spectra from Varian 800MHz at 25°C of different GAG standards: (A) bovine tracheal chondroitin sulfate A (CS-A), (B) shark cartilage chondroitin sulfate-C (CS-C), oversulfated chondroitin sulfate (OSCS), (D) dermatan sulfate (DS), or chondroitin sulfate-B, and (E) heparan sulfate (HS), dissolved in 50 mM acetate buffer 12.5% D_2O (pH 4.5) 0.1 % sodium azide, at a final 15 mg/mL concentration. Reproduced from [10].

Note that through ^{15}N -HSQC spectroscopy, all GAG standards show just the ^1H - ^{15}N cross-peak related to their differential hexosaminy units, in a very simple way that allows rapid structural assignments. Although the NMR peaks are few, these resonances are still quite useful for structural determination in glycosaminoglycanomics. All signals from different standards are characteristic, and resonate with distinct ^1H - or ^{15}N -chemical shifts (Figure 4) [10]. Structural features such as the hexosaminy type (galactosamines at upfield ^1H - and ^{15}N -chemical shifts, Figures 4A-D, as opposed to glucosamines at a more downfield ^1H - and ^{15}N -chemical shifts, Figure 4E), sulfation pattern (4-sulfation at the upfield ^{15}N -chemical shifts, Figures 4A, B and D, as opposed to more downfield ^{15}N -chemical shifts of 4,6-disulfated units, Figure 4C, and further more downfield ^{15}N -chemical shift of 6-sulfated units, Figure 4A, and B), and adjacent uronic acid type (glucuronic acid at upfield ^1H -chemical shifts, Figures 4A-C, as opposed to iduronic acid at the more downfield ^1H -chemical shifts, Figure 4D) can be easily determined through this method [10]. These studies concerning the use of ^{15}N -NMR for structural characterization in GAG molecules turned out to be quite valuable also in predicting the anomericities in GAG-derived oligosaccharides as well as the sulfation patterns. For more details read reference 10 about this topic.

One downside of the ^{15}N -NMR application on structural studies of GAGs is the very fast exchange rates of protons from sulfamate groups (NHSO_3^-) that are quite abundant in glucosamines of certain GAG types, such as heparan sulfates and heparins. Although the ^1H - ^{15}N cross-peaks from ^{15}N -HSQC spectra of residual N-acetylated glucosamines (GlcNAc) can be fairly used to quantify the amounts and types of uronic acid units, to which GlcNAc are linked (Figure 5), the remaining amounts of uronic acids linked to N-sulfated glucosamines (GlcNS) can be missed under normal conditions. Alternative ways to force the protonated states in sulfamate groups is the use of controlled samples at narrow pH range (7.0-8.0) [15], or to slow down the fast ^1H -amide exchange rates recording experiments at very low-temperatures, as detailed next with preliminary results using commercially available sodiated GlcNS as a molecular model to mimic the composing N-sulfated amino sugars in heparins and heparan sulfates.

Very low temperatures such as 3°C (20% acetone is added to avoid freezing) can slow down considerably the solvent exchange of the labile protons. All protons, inclusively the exchangeable ones from sulfamate or hydroxyl groups of GlcNS, become thus detectable by ^1H -based NMR spectroscopy (Figure 6A). This can be exemplified with the 1D spectrum of GlcNS at Figure 6A. The ^1H -peaks can be assigned through spin-systems from TOCSY spectrum using this same hydrated low-temperature condition (Figure 7A), like the same way undertaken and explained for Glc (Figure 2). The α - and β -anomers with ^1H -chemical shifts respectively at ~ 5.42 and ~ 4.68 ppm (Figures 1 and 6A) serve as starting point for tracing connectivities by cross-peaks in TOCSY spectrum also recorded in water-rich solution (Figure 7A). They have $^3J_{\text{H1-H2}}$ respectively around ~ 3.17 and ~ 2.98 ppm (Figure 7A). These H2 resonances have consequently further connections with ~ 5.33 and ~ 5.86 ppm, respectively for α - and β -anomers. The latter ones are amide protons with chemical shifts determined for further assignments in ^{15}N -HSQC spectrum. These signals were not observed in the protonated amide condition (data not shown). Using the hydrated and cold condition, the ^{15}N -HSQC spectrum (Figure 7B) turns now to be useful in detection of the

protonated state of sulfamate groups, and the ^1H - ^{15}N cross-peaks of each NH are at the expected chemical shifts as seen by TOCSY spectrum (Figure 7B). Note that in the ^{15}N -HSQC spectrum, the amides anomeric showed swapped ^1H -chemical shifts, since the α -form of GlcNS is the predominant population in solution (Figure 1).

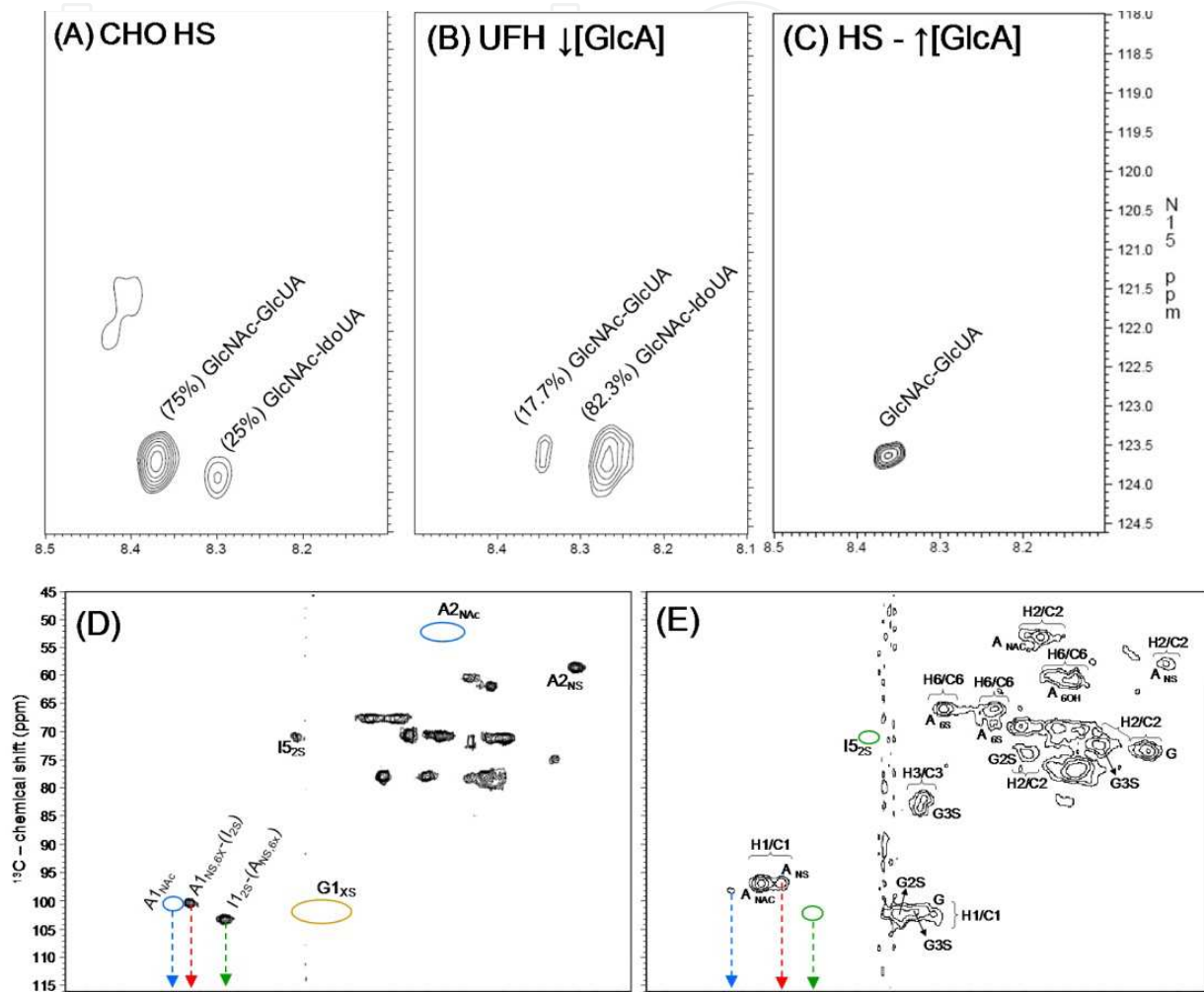


Figure 5. ^{15}N - (A-C) and ^{13}C - (D, E) HSQC spectra of heparan sulfate (HS) (A, C, and E) and unfractionated heparin (UFH) (B, D), recorded at Varian 800 MHz (A-C) and Bruker 400 MHz (D, E). The HS in panel A was from cultures of chinese hamster ovarian (CHO) cells [10], the UFH in panel B was from a pharmaceutical supplier, and the HS in panel C was extracted from the bivalve *Nodipecten nodosus* [16]. Note that the (B) UFH and (C) HS have respectively low and high amounts of glucuronic acids (GlcUA), as demonstrated by the tiny or missing color-coded peaks in their respective ^{13}C -HSQC spectra of panels D and E. In these panels, the letters used are A for glucosamine, I for iduronic acid, G for glucuronic acid, NAc for N-acetyl, NS for N-sulfation, 6X for 6-(un)substituted, 2S for 2-sulfation, XS for 2- and/or 3-sulfation, and 3S for 3-sulfation. The number right after the capital letters designate the ring position, for example, I5_{2S} means a cross-peak of the ^1H - ^{13}C pair at the 5-position of a 2-sulfated iduronic acid ring. Hence, the colors indicate blue for N-acetyl glucosamines, red for N-sulfated glucosamines, green for iduronic acids, and yellow for glucuronic acids.

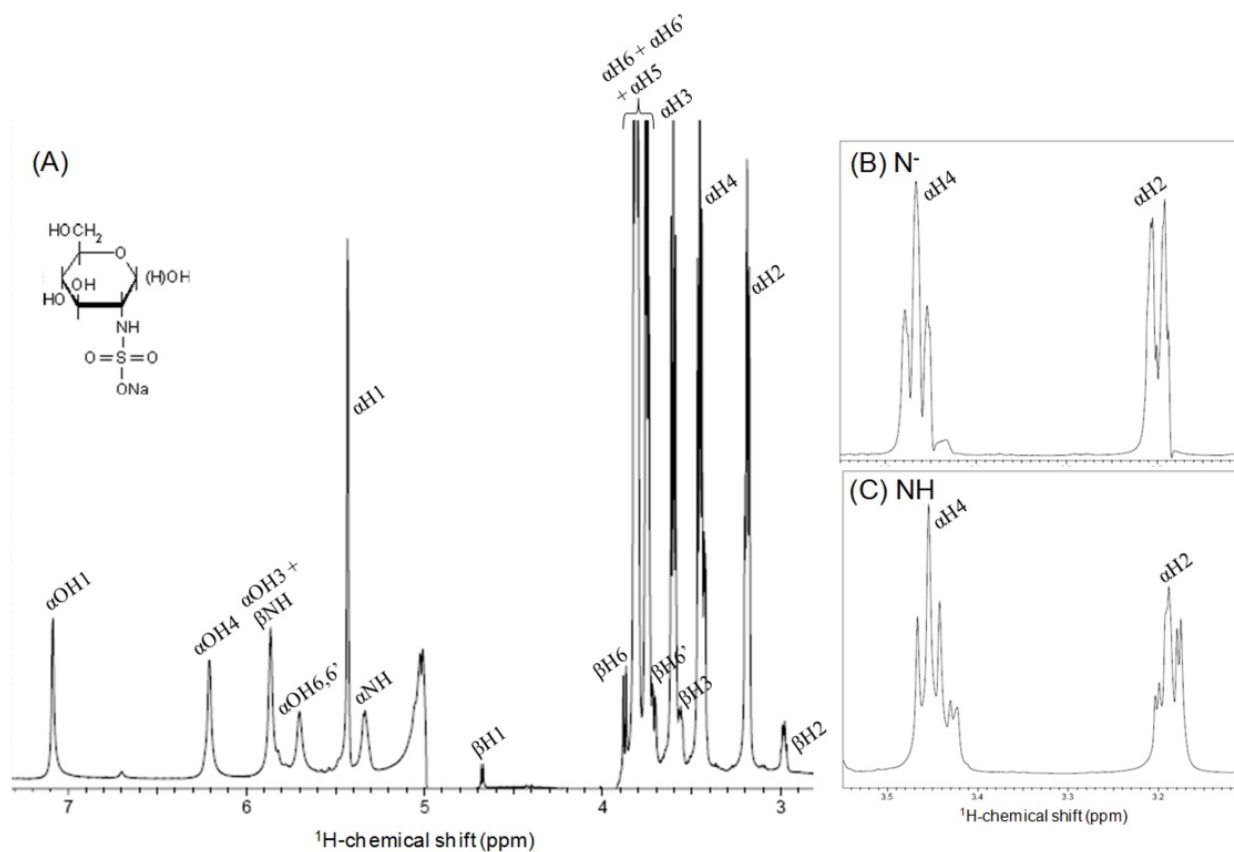


Figure 6. 1D ^1H -NMR expansions 2.8-7.3 ppm (A) and 3.10-3.55 ppm (B, C) of 5 mg/mL GlcNS in 10:20:70% D_2O :Acetone: H_2O (pH 4.5) at 3°C (A, C) and at 15°C (B) in spectrometer Varian 800 MHz. Note that in panel B, the resonance of $\alpha\text{H}2$ splits in a dublet of dublets due to $^3J_{1\text{H}2-1\text{H}1}$ and $^3J_{1\text{H}2-\text{H}3}$, while in panel C there are a triplet of dublets for the split of $\alpha\text{H}2$ due to $^3J_{1\text{H}2-1\text{H}1}$, $^3J_{1\text{H}2-\text{H}3}$, and now the $^3J_{1\text{H}2-\text{HN}}$ since in the former case the amide is deprotonated because of the higher temperature, but in case of panel C, the amide is protonated because of lower temperature. The structure of the GlcNS in its protonated and sodiated state is shown on the top left side of the panel A.

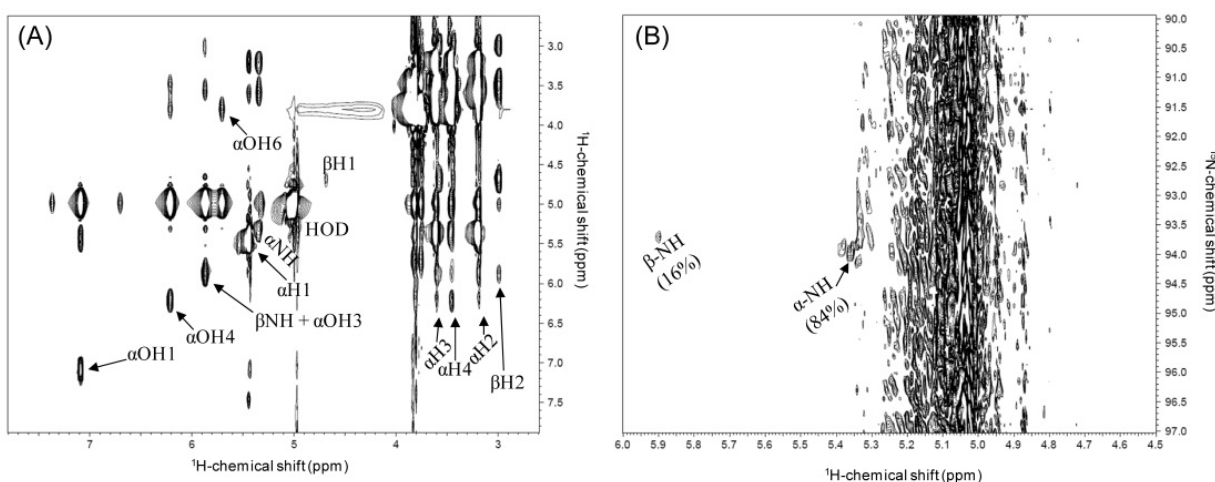


Figure 7. (A) TOCSY and (B) ^{15}N -HSQC spectra of GlcNS, at 3°C , in a Varian 800 MHz. The exchangeable protons from hydroxyl and amide groups are accordingly labeled. The population percentage of the anomeric forms are indicated in panel B. The α -anomers of GlcNS are more populated as seen in Figure 1.

2.3. Examining flexibility and dynamic properties of glycans by relaxation rates measurements

In radio-frequency pulsed NMR experiments, the magnetization aligned with the static magnetic field (B_0) is tilted away from the longitudinal Z -axis (parallel to the static magnetization), and placed into the X,Y -transverse plane. The fundamental property that brings back the magnetization to the Z -plane, restoring therefore the equilibrium during this modern pulsed NMR experiments is the spin relaxation phenomena [17]. The relaxation mechanisms are particularly dependent of the molecular motions of either internal localized sites or the overall tumbling of the molecule in solution. Therefore, relaxation measurements are very useful for studying molecular dynamic processes on a fast time scale. The longitudinal or spin-lattice relaxation process is given by the relaxation time T_1 , and this is a measure of how fast the longitudinal magnetization goes back to its original state before the pulses. The transversal or spin-spin relaxation effect denoted by the time course T_2 , measures how fast the Free Induction Decay (FID) dissipates its magnitude from the X,Y -transverse plane. Several mechanisms are known to influence the T_2 relaxation time, such as the dipolar interactions like dipole-dipole and dipole-chemical shift anisotropy [17]. The relaxation rates (R_1 and R_2) measurements (in ms to s) are the inverse of T_1 and T_2 respectively. As discussed below using some published data from the literature, these rates and thus relaxation times, combined with measurements of line-widths or line broadening (in Hz) during NMR experimentation, can be successfully used for determine dynamic properties of either free glycans in solution as glycan domains of glycoconjugates.

In a recent study about structural dynamics of the saccharidic portion of immunoglobulin G (IgG) using NMR spin-relaxation [18], the authors have proved that both glycan branches at the Fc fragment (Figure 8) are accessible and dynamic in solution. This motion, and glycosylated rates (Figure 8) are responsible to participate during the cellular responses of the adaptive immune systems, mainly modulating the health balance between hyposensitivity to foreign particles versus hypersensitivity to auto-antigens. Again, the spin labeling technique as discussed in section 2.2 was crucial to advance this work. In this reference, the N-glycan at Asparagine-297 was enzymatically remodeled by sialyltransferases and glycosidases to build up branches specifically labeled with ^{13}C -isotope in galactosyl units (Figure 8). This initial procedure of spin labeling indicated already an apparent accessibility of these branches to the remodeling activity of the enzymes, unlikely previous conceptions of a more static and internalized behavior of these branches. As discussed next, the spin relaxation measurements of these branches have ultimately confirmed these dynamic properties [18].

NMR resonance linewidths (half-height of the peak, in Hz), which are directly related to the transverse relaxation rates (R_2 values) are values indicative of dynamic properties. Narrow lines indicate decreased relaxation rates and thus increased rates of rotational motions. The linewidths of the ^{13}C -labeled galactose in the α 1-6Man branch was over three-times that of the corresponding resonance from the α 1-3Man branch (Table 3) [18]. This suggested that the α 1-6Man branch is considerably more immobilized than the other antennary. At

experiments undertaken at higher fields, the ^{13}C linewidths of the $\alpha 1\text{-6Man } ^{13}\text{C}2$ resonance of galactose gave values more than three-times than the correspondent on the other branch. Interpretation using an isotropic model gave an effective correlation time of 37 ns, which is considerably longer than the hydrodynamic predictions for the Fc fragment, and the protein tumbling time (~ 20 ns). This suggested that although the $\alpha 1\text{-6Man}$ branch is partially immobilized, there should be still some dynamic properties of this branch to explain the higher experimental value. Therefore a more complete set of relaxation time was measured at two different magnetic strengths (Table 3). A field-dependent R_2 values were obtained, with smaller relaxation at 14.0 T (600 MHz) as opposed to 21.1 T (900 MHz). All R values combined at the lower magnetic field were not consistent with prediction based on isotropic tumbling model and have suggested that if the relaxation were solely dipole in origin, R_2 would be even less at this field strength [18]. Both the field dependence and these inconsistencies have suggested contribution from chemical exchange contributions to R_2 relaxation mechanisms that originated from the $\alpha 1\text{-6Man}$ branch sampling multiple conformational states on the microsecond to millisecond timescale and therefore, modulating chemical shift in this process. At least, some of these states have to have substantial internal motion to raise the rotational R_1 value (R_{1p}).

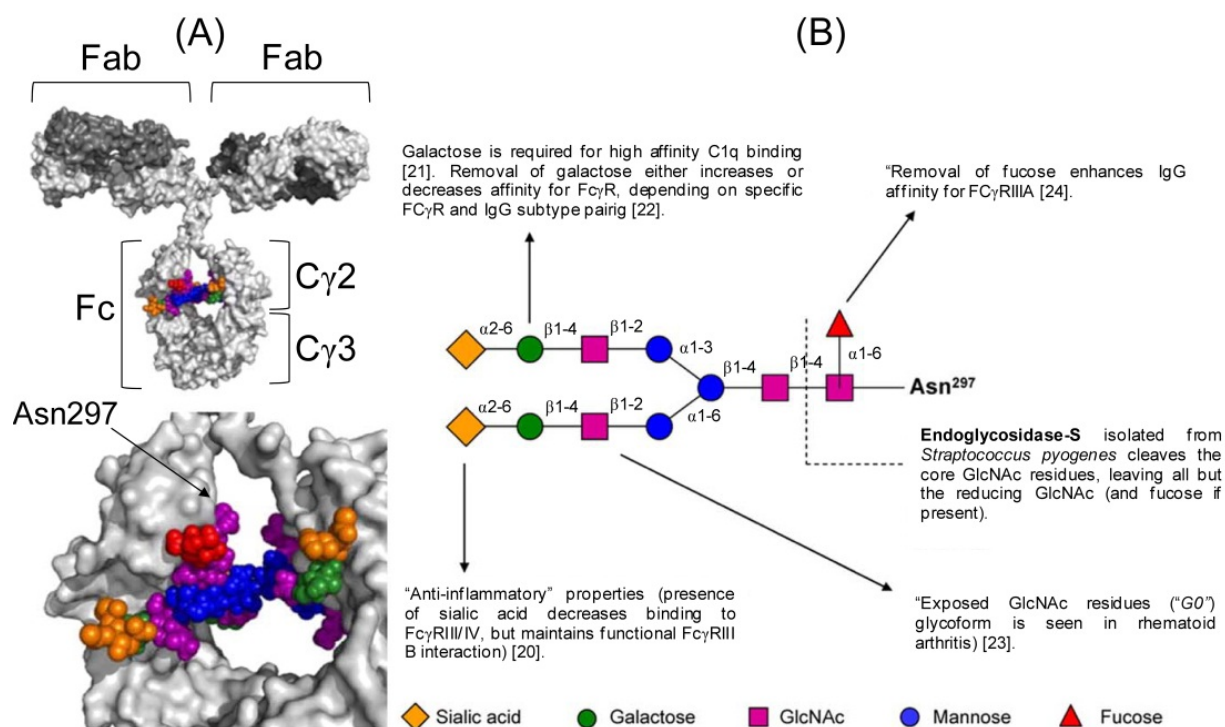


Figure 8. The conserved N-linked carbohydrate domain of IgG is attached to Asn-297 of the C γ 2 domains of each IgG heavy chain. Data modified from [19]. A range of other glycoforms (full or partial unsialylated and/or ungalactosylated) also exists on serum IgG [19]. These other glycans are based mostly on the biantennary structure but without some or all of the sialic acid or galactose residues from the non-reducing terminus (or fucose residues from the core). The presence of a particular carbohydrate maintains a defined structure of the Fc region that leads to specific consequences for the Fc function. Some of the key glycan-mediated interactions with receptors, for example, are indicated and properly referenced [20-24]. Heavy and light chains are colour-coded in light and dark grey respectively.

	α1-3Man-linked	α1-6Man-linked
	Relaxation rates	Relaxation rates
900 MHz	Galactose $^{13}\text{C}6$	Galactose $^{13}\text{C}6$
R_1	$2.8 \pm 0.1 \text{ s}^{-1}$	$3.1 \pm 0.4 \text{ s}^{-1}$
R_2	$48.4 \pm 5.5 \text{ s}^{-1}$	$59.7 \pm 9.2 \text{ s}^{-1}$
900 MHz	Galactose $^{13}\text{C}2$	Galactose $^{13}\text{C}2$
R_1	$1.2 \pm 0.1 \text{ s}^{-1}$	$1.2 \pm 0.2 \text{ s}^{-1}$
R_{1p}	$20.1 \pm 1.0 \text{ s}^{-1}$	$56.1 \pm 10 \text{ s}^{-1}$
R_2 linewidths	40 s^{-1}	150 s^{-1}
600 MHz		
R_{1p}	$14.7 \pm 1.1 \text{ s}^{-1}$	$48.0 \pm 5.4 \text{ s}^{-1}$
R_2 linewidths	28 s^{-1}	107 s^{-1}
R_2	29 s^{-1}	ND

ND, not determined owing to low signal-to-noise ratio.

* Reproduced from [18].

Table 3. ^{13}C relaxation measurements of galactose residues from Fc isotopic labeled at either C2 or C6 positions.

In order to probe the existence of chemical exchange contribution, relaxation dispersion experiments can be employed, in which transverse relaxation rates (R_2) can be measured using Carr-Purcell-Meiboom-Gill (CPMG) pulse sequences [25]. Through this NMR experiment type, resonances that experience multiple chemical environments on a timescale near to ν_{CPMG} (variable pulsing rates due to varying delays between the forming 180° pulses of CPMG pulse sequences) must become more intense as a function of increasing pulsing rates. Results from this experiment using both α 1-3Man and α 1-6Man branches of IgG Fc with ^{13}C -labeled galactose residues at 50° C , and at two different magnetic strengths (21.1 T, 900 MHz, and 18.8 T, 800 MHz) have shown this profile (Figure 9). At low pulsing rates, the relaxation measurements approach predictions using linewidths. At higher pulsing rates, chemical shifts are canceled out due to rapid chemical shift refocus, therefore chemical exchange contributions can be sorted out. Clearly, the R_2 values of α 1-6Man branch decrease with pulsing rates, whereas the values for the other branch have kept constant (Figure 9A). The change in R_2 in the presence of chemical exchange between two states (A and B) was described using the equation $R_2(1/\tau_{\text{cp}}) = R_2^0 + \phi_{\text{ex}}/k_{\text{ex}} [1 - 2 \tanh(k_{\text{ex}}\tau_{\text{cp}}/2)/k_{\text{ex}}\tau_{\text{cp}}]$, where $\phi_{\text{ex}} = P_A P_B \Delta\omega^2$, R_2^0 is the relaxation rate in the absence of chemical exchange, k_{ex} is the exchange rate, τ_{cp} is the delay between refocusing pulses, and $\Delta\omega^2$ is the frequency difference of states A and B in angular units [26]. Through this equation, the contribution of chemical exchange to the observed R_2 was seen to depend on the rate of exchange, the time between pulses and the scaling factor ϕ_{ex} . Fitting this equation to the data that was obtained for the α 1-6Man branch, an effective exchange constant (k_{ex}) of $5,300 \pm 1,700 \text{ s}^{-1}$ was generated [18]. The scaling factor ϕ_{ex} in principle can yield information about the nature of the exchange process by describing populations of states and chemical shift changes on moving between states. The ϕ_{ex} at 21.1T and 18.8 T were respectively, $380,000 \pm 60,000 \text{ rad}^{-2} \text{ s}^{-2}$, and $300,000 \pm 100,000 \text{ rad}^{-2} \text{ s}^{-2}$. The R_2^0 for each magnetic field were respectively $26 \pm 13 \text{ s}^{-1}$, and $39 \pm 7 \text{ s}^{-1}$ [18].

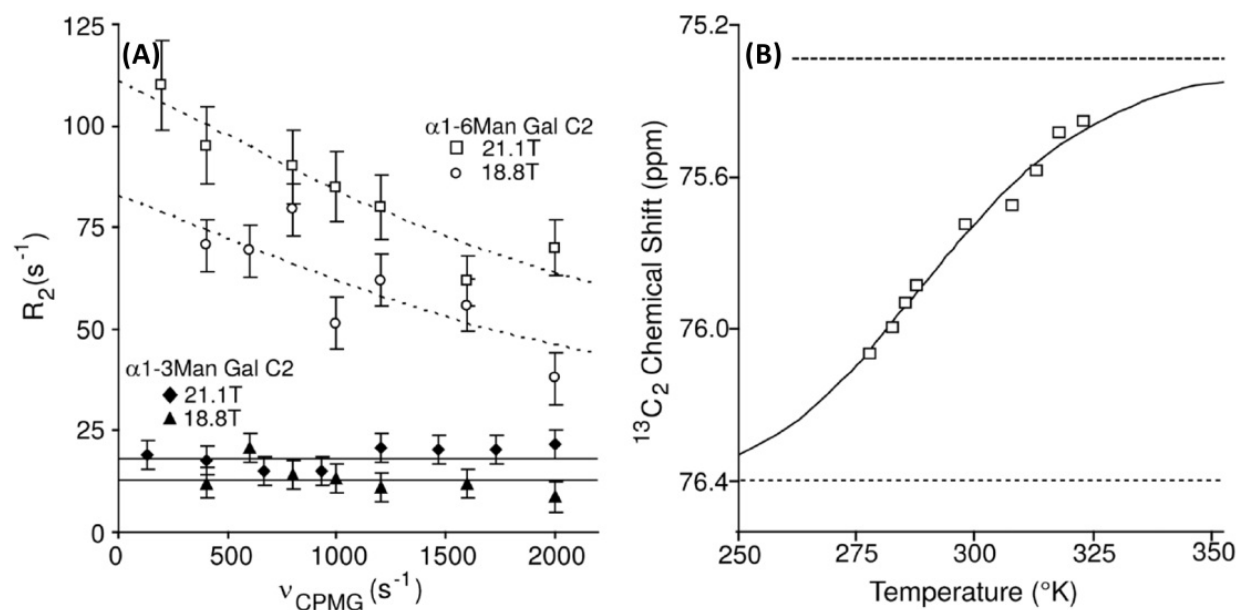


Figure 9. (A) Relaxation dispersion and (B) temperature-dependent chemical shift measurements show evidence of two states (A and B). (A) The relaxation dispersion experiments indicate motion at the micro-millisecond timescale for the $\alpha 1$ -6Man branch but not for the $\alpha 1$ -3Man branch. (B) The chemical shift of the $\alpha 1$ -6Man branch-linked $^{13}\text{C}_2$ -galactose approaches a saturation point at higher temperatures and permits the estimation of chemical shift values for two states. Chemical shift asymptotes for high-temperature (state A) and low-temperature (state B) are represented with discontinued lines. Reproduced from [18].

The effects of chemical exchange rates on R_2 can be also investigated using the rotational spin lattice-relaxation ($R_{1\rho}$) measurements. $R_{1\rho}$ of both branches (Table 3) approach the rapid pulsing limit of R_2 in CPMG experiments (Figure 9), which represents the approaching to a non-exchange contribution to R_2 . The large deviation seen for the $\alpha 1$ -6Man branch is consistent with the considerable chemical exchange contribution. Taking all these relaxation-based data, two conformational states were observed for $\alpha 1$ -6Man branch: one related to chemical exchange contribution within contact with the peptide chain, and another regardless the molecular contact resulted from low chemical exchange contributions [18]. Taking together the existence of these both states, a dynamic behavior for the $\alpha 1$ -6Man branch has been proved, while the constant low chemical exchange contribution of $\alpha 1$ -3Man branch has pointed towards a glycan segment more externalized from the $\text{C}\gamma 2$ domain (Figure 8). These conclusions will be sustained by other results about chemical shift changes [18], as described in the following item.

2.4. Applications and implications of chemical shifts in glycobiology

Chemical shift values (δ , in ppm) together with coupling constants comprise the major information extracted in NMR studies of proteins and nucleic acids [27], and thus are of great usefulness in glycobiology as well. Chemical shift values provide reliable information concerning the chemical environments in which a given atom (nucleus) molecularly experiments at certain timescale. If there were no other kinds of interactions in addition to

the Zeeman interaction [28] during the NMR experimentation, all nuclei of a given molecule would lead to the same frequency in a 1D NMR spectrum. Zeeman states represent the two spin possibilities of a spin-half nucleus (usually defined as α - and β -spin states) under the static magnetic field (B_0) [29]. Due to changes on the chemical environment of the nucleus within the molecules chemical shifts may experience different values which will result different frequencies even though the same isotope and with same Larmor frequency. One of the major determinants in the chemical shifts is the electronic shielding generated by the electrons that surround the spin-half nuclei. Electrons at these surrounds have also angular momentum and thus magnetic moment. Differential conformational states may give different chemical shift values in a limited time-range. This can be explored to understand dynamic behaviors of glycans and to understand the chemical structures of biomolecules. Another application in the exploration of chemical shift changes is in glycan-involved intermolecular complexes, such as those of carbohydrate-binding proteins. The former phenomenon will be briefly explained through the dynamic properties of the α 1-6Man branch of IgG Fc [18], continuing the same example taken at the previous section. The latter phenomena on concerning intermolecular complexes involving carbohydrate-binding proteins and glycans as common ligands will be discussed afterwards, taken some unpublished data about the binding properties of the chemokine RANTES complexed with chondroitin sulfate hexaccharides of well-defined sulfation patterns.

2.4.1. The dynamic behavior of glycans through chemical shift changes: the bound and unbound states of the N-glycan of IgG Fc

The chemical shifts of the Fc α 1-6Man galactose residue were observed to be clearly temperature-dependent (Figure 9B). The ^{13}C 2-resonance can show a significant displacement between 5-50°C with its ^{13}C -chemical shift trending toward a plateau of 75.3 ± 0.2 ppm at the high-temperature limit (Figure 9B) [18]. This plateau value is quite consistent with chemical shift values from the free glycan in solution which implies that the glycan is far away from chemical environment promoted by the Fc amino acids (state A, Figure 10). Although Figure 9B showed a curve-fitting only for the C2 resonances, the ^{13}C 6-chemical shift showed a similar trend and moved from a perturbed resonance position at lower temperatures towards a free glycan position at higher temperatures [18].

Through the use of the chemical shift values determined for state A in conjunction with the observed chemical shifts at 50°C obtained from CPMG relaxation dispersion data, the 0.8 value was extracted for the state A population (P_A) using the equation $P_A = 1/[\omega^2(\delta_X - \delta_A)^2/\varphi_{\text{ex}}] + 1$. Then the P_A value was used to deconvolute φ_{ex} and derive a value for $\Delta\omega$ using the relationship of $\varphi_{\text{ex}} = P_A P_B \Delta\omega^2$. The determined chemical shift for state B was therefore 76.4 ± 0.5 ppm using the resultant value for $\Delta\omega$ of $1,500 \pm 300$ rads^{-1} along with the state A chemical shift. Moreover, the data obtained have indicated that populations of both states are nearly equal at 15°C and shift towards higher population of state A (the state with chemical shifts similar to free glycans in solution) at temperatures higher than 15°C. At body physiological temperature state A is approximately 70% populated.

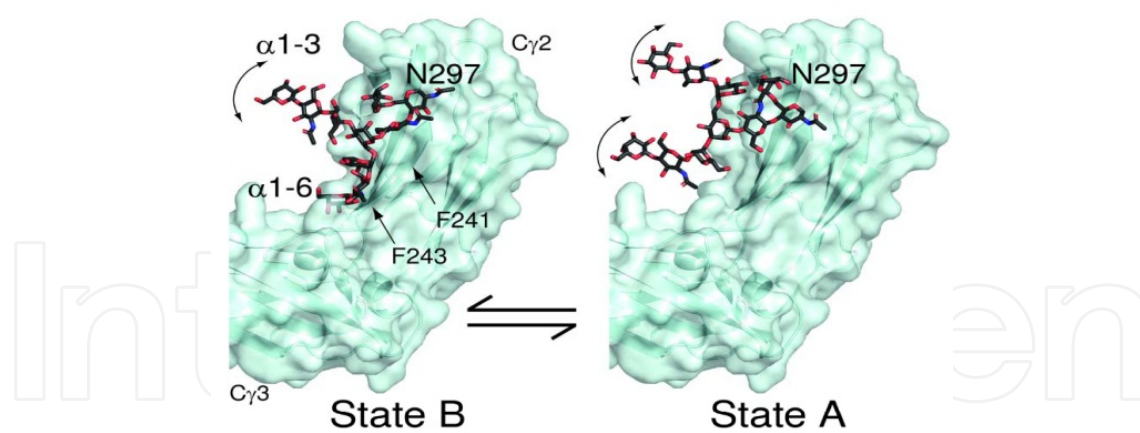


Figure 10. Models for Fc N-glycan dynamics and accessibility showing that exposed conformational states of branches are possible. While the α 1-3Man branch is highly flexible out of the protein pocket, the α 1-6Man branch is partially dynamic within two states: externalized A state *versus* internalized B state. Reproduced from [18].

2.4.2. Unveiling binding sites of carbohydrate-binding proteins through chemical shift perturbation: The chemokine CCL5/RANTES-chondroitin sulfate hexasaccharides complexes

Chemokines are a family of small cytokines with chemotactic properties. They are small and soluble proteins (with a mass of 8-16 kDa), and are produced and released by a variety of cell types during the initial phase of host responses to injury, allergens, antigens, or invading microorganisms. Chemokines share a sequence homology and possess four cysteines in conserved locations. These form two disulfide linkages that are keys to their tertiary structure and stability (Figure 11). These cysteines are also involved in the nomenclature and classification of the chemokines. Among many chemokines, CCL5, also known as RANTES, is a 68-residue proinflammatory chemokine responsible to control migration and trigger activation of leukocytes during their trafficking to the inflamed sites. Both these biological activities of CCL5 have shown to be critically influenced by interactions with GAG in endothelial surface proteoglycans [30]. The immobilization of the CCL5 onto surface proteoglycans will attract leukocytes to the sites of injury, helping the rolling step which is heavily driven by selectin-mediated interactions; followed by the activation step of the leukocytes. This step is driven by the interaction of the CCL5 receptor on the leukocyte (CCR5) with the immobilized CCL5. GAGs in proteoglycans do not only regulate these two steps but also induce the oligomerization of CCL5 [31]. This GAG-induced oligomerization process is crucial to i) create a high local concentration of chemokine to optimize the chemoattraction of cell for sites of lesion, ii) increase the *in vivo* CCL5 half-life due to enhancement of protection from natural proteolysis, iii) promote resistance to physical disruptions caused by the blood flow in vessels, and iv) serve as storage resources for rapid mobilization of chemokines without biosynthesis [31]. Recently, the GAG-induced oligomeric structure of CCL5 was revealed by NMR, MS and small-angle X-ray scattering (SAXS) experiments [32]. Although, the heparin binding site of CCL5 has already been reported [33], comprising the segment ⁴⁴RKNR⁴⁷, the potential GAG binding sites of CCL5 are yet undocumented, especially considering chondroitin sulfate which is the most abundant GAG in the human body, and widely spread across surface proteoglycans of blood vessels.

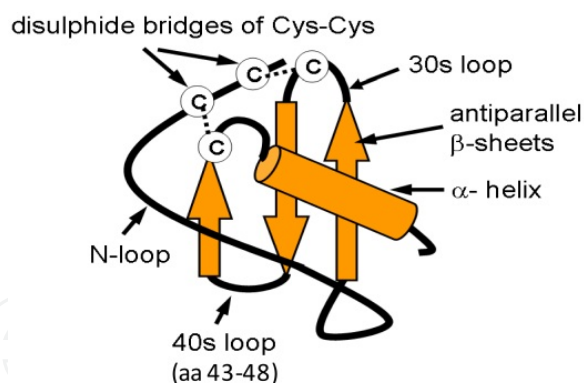


Figure 11. 3D structural model of the CC chemokines.

The ^{15}N -HSQC spectrum of the ^{15}N -labeled E66S CCL5 (Figure 12), which is mostly found as monomers in solution rather than the oligomerization propensity of the wild type [35], showed well-resolved amide signals that allowed easily a near-complete chemical shift assignment (Table 4). These initial assignments are crucial to further inform the chemical shift changes induced by the presence of increasing concentration of the ligands. The ligands used were two chondroitin sulfate hexasaccharides fully characterized by NMR [34]. They are named CS 6-6-4, and CS 4-4-4, which represent the following respective structures: $\Delta\text{UA}(\beta 1 \rightarrow 3)\text{GalNAc}6\text{S}(\beta 1 \rightarrow 4)\text{GlcA}(\beta 1 \rightarrow 3)\text{GalNAc}6\text{S}(\beta 1 \rightarrow 4)\text{GlcA}(\beta 1 \rightarrow 3)\text{GalNAc}4\text{S-ol}$, and $\text{GlcA}(\beta 1 \rightarrow 3)\text{GalNAc}4\text{S}(\beta 1 \rightarrow 4)\text{GlcA}(\beta 1 \rightarrow 3)\text{GalNAc}4\text{S}(\beta 1 \rightarrow 4)\text{GlcA}(\beta 1 \rightarrow 3)\text{GalNAc}4\text{S-ol}$. The abbreviations are ΔUA for $\Delta^{4,5}$ unsaturated uronic acid; GalNAc for N-acetyl galactosamine; GlcA for glucuronic acid; "S" for sulfation group, digits before "S" represent the ring position; and -ol stands for reduced sugars (open rings at the reducing-end terminal units) [34].

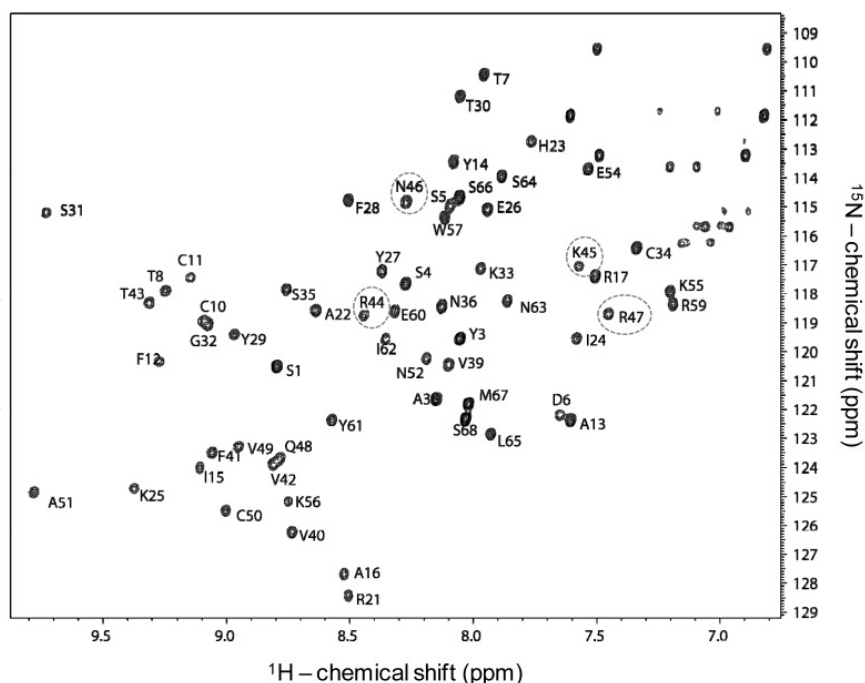


Figure 12. ^{15}N -HSQC spectrum of the ^{15}N -labeled E66S chemokine CCL5/RANTES (1-2 mM) in 150 mM sodium acetate buffer, pH 4.5. The amide signals are labeled accordingly to their respective amino acids. The signals circled in grey represent the heparin motif binding site (BBXB) [33].

Residue	¹⁵ N (ppm)	NH (ppm)	Residue	¹⁵ N (ppm)	NH (ppm)
S1	120.50	8.78	S35	117.88	8.74
P2	nd*	nd	N36	118.49	8.11
Y3	119.64	8.04	P37	nd	nd
S4	117.76	8.26	A38	121.67	8.14
S5	114.91	8.07	V49	120.49	8.08
D6	122.29	7.63	V50	126.32	8.72
T7	110.44	7.94	F41	123.53	9.04
T8	117.88	9.22	V42	124.07	8.81
P9	nd	nd	T43	118.28	9.31
C10	118.92	9.08	R44	118.69	8.43
C11	117.50	9.13	K45	117.01	7.57
F12	120.36	9.26	N46	114.91	8.24
A13	122.35	7.59	R47	118.63	7.43
Y14	113.41	8.07	Q48	123.72	8.78
I15	124.00	9.09	V49	123.30	8.92
A16	127.69	8.51	C50	125.46	8.99
R17	117.39	7.50	A51	124.84	9.76
P18	nd	nd	N52	120.24	8.16
L19	nd	nd	P53	nd	nd
P20	nd	nd	E54	113.87	7.52
R21	128.41	8.49	K55	117.89	7.19
A22	118.62	8.62	K56	127.69	8.51
H23	113.15	7.73	W57	115.25	8.08
I24	119.62	7.56	V58	122.48	5.61
K25	124.73	9.36	R59	118.49	7.17
E26	115.13	7.92	E60	118.62	8.29
Y27	117.14	8.35	Y61	122.35	8.54
F28	114.78	8.48	I62	119.62	8.34
Y29	119.40	8.96	N63	118.25	7.84
T30	111.25	8.03	S64	114.02	7.86
S31	115.27	9.71	L65	122.97	7.90
G32	119.08	9.06	S66	114.77	8.04
K33	117.13	7.95	M67	121.86	8.00
C34	116.51	7.32	S68	122.52	8.02

*not determined.

Table 4. ¹⁵N and ¹H chemical shift of E66S at 297K, pH 4.5. The amino acids that form the heparin binding site motif (BBXB) are highlighted in bold.

As the concentration of the chondroitin sulfate ligands increases, either loss of signal intensity or chemical shift migration were observed on the ^{15}N -HSQC spectra of E66S CCL5 (Figure 13). In the case of the continuous titration using the ligand CS 6-6-4 (left-hand side spectrum of Figure 13), the signal intensity decreases proportionally, and no chemical shift migration was seen. This likely indicates a slow exchange rate between the on- and off-states of the complex, and the GAG-induced oligomerization was observed since large amounts of precipitates were visually formed on the bottom of the NMR tube during the titration experiment (data not shown). This precipitation phenomenon is one of the major reasons for the NMR signal intensity loss. Conversely, the titration using the ligand CS 4-4-4, no intensity loss was observed even using 10 equivalent molar of this ligand (blue spectrum), and clear chemical shift migration of certain peaks was observed (right-hand side spectrum of Figure 13). In the experiment using this ligand, the amino acids that showed the major chemical shift changes were S1, Y3, D6, T7, R17, K45, N46, R47, Q48, as indicated in the spectrum of Figure 13. The residues K45, N46, and R47 match perfectly with the heparin binding motif (Table 4) [33]. These residues that experience the largest chemical shift migration are highlighted on the structure of CCL5, represented in both cartoon and surface structural models (Figure 14). They are located at the pocket of the dimer consisted of the 40s loop, which in turn includes the heparin binding motif, together with the N-terminal (Figure 11).

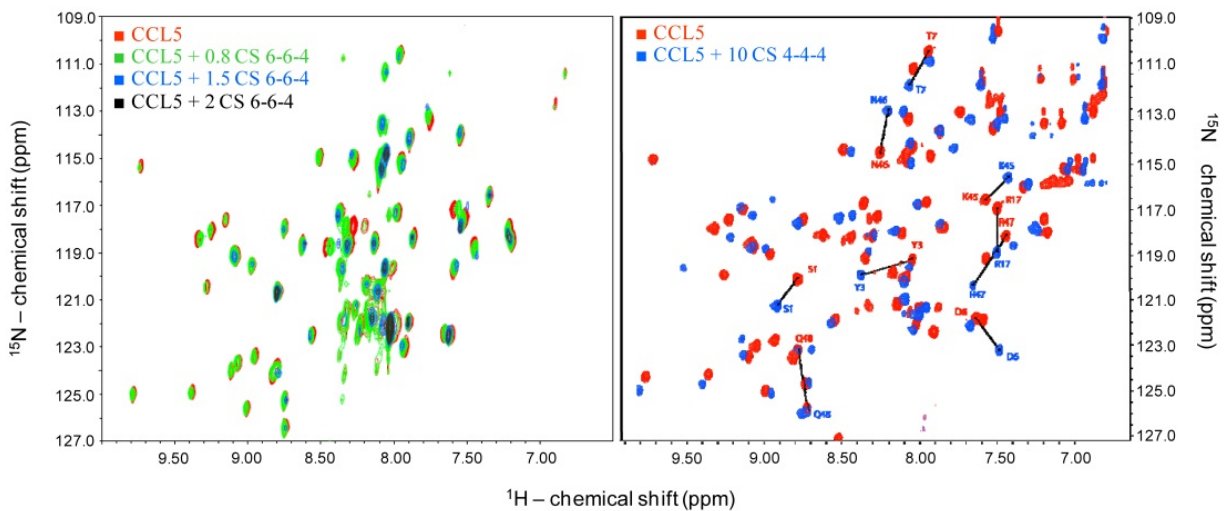


Figure 13. Superimposed ^{15}N -HSQC spectra from ligand titration on CCL5 in solution. The ligand types and relative concentration to the protein are indicated and color-coded as shown on the panels.

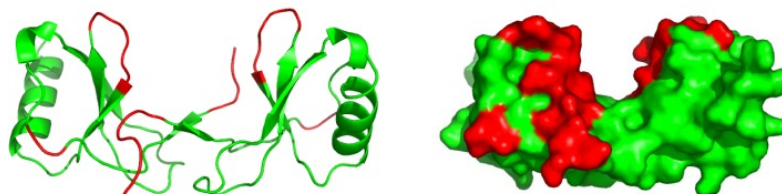


Figure 14. Cartoon (left) and surface (right) models of CCL5. In red are the amino acid S1, Y3, D6, T7, R17, K45, N46, R47, Q48 that have experienced the largest chemical shift migration induced by the presence of the ligand CS 4-4-4.

In order to understand the physiological condition of the GAG-induced oligomerization of CCL5 promoted by the CS 6-6-4, and the nature of the binding involved in the interaction between these two molecules, an experiment using increasing concentrations of sodium chloride was performed (Figure 15) at the 2-times molar excess of ligand. This was the condition that showed the huge precipitation and loss of signal intensity (black spectrum at left panel of Figure 13). It is clearly observed that at physiological salt concentration (150 mM NaCl) the low intensity of CCL5's signals still indicate oligomerized states of the chemokine. However, this highly-complexed state is broken down at higher salt molar concentrations than the physiological condition as seen with the recovery of the signal intensity in the spectrum with 300-450 mM. This result indicates that only at higher salt concentrations than the physiological condition, the oligomerization of CCL5 is abrogated and the nature of the binding between the two molecules is just electrostatic. The return in loss of the signal intensity in the ^{15}N -HSQC spectra of CCL5 is just consequence of an instrumentation limitation due to the extreme high salt molarity that disturbs the magnetization sensitivity on the probe (the detection devise of the magnet). In synthesis, the CS 6-6-4 induces CCL5 aggregation whereas CS 4-4-4 just a little. This preliminary result indicates that the oligomerization of this chemokine is triggered by specific regions of the GAG chains in endothelial surface proteoglycans.

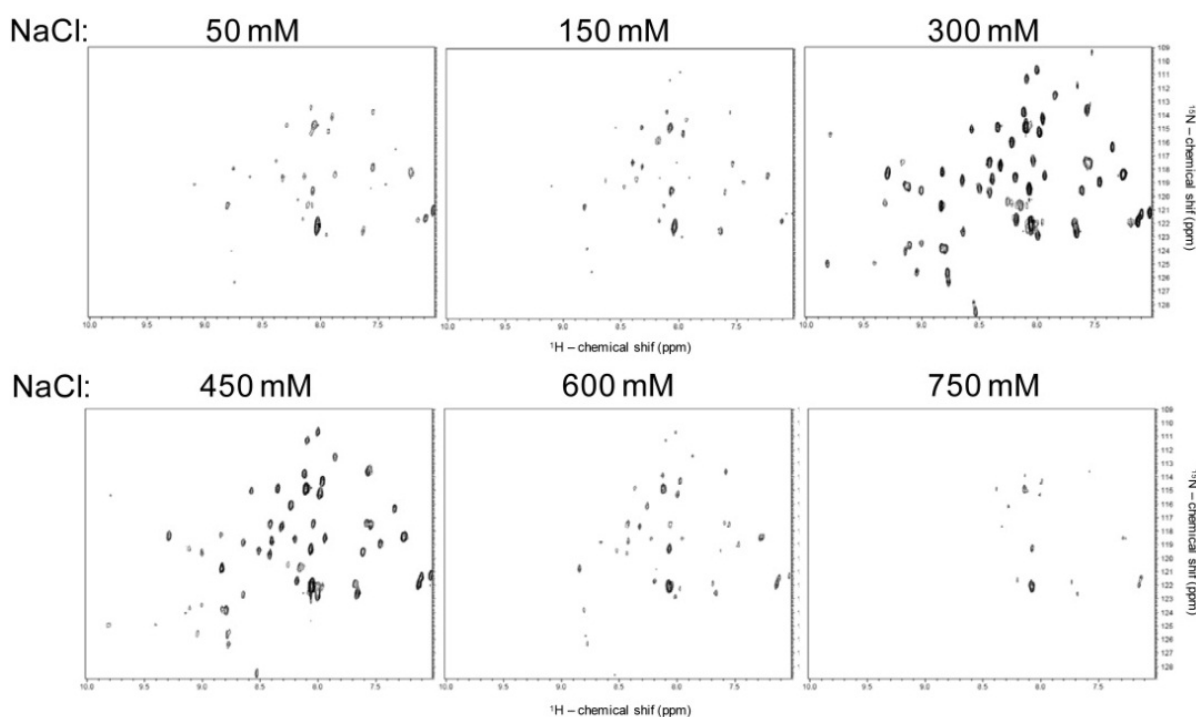


Figure 15. ^{15}N -HSQC spectra of CCL5 with 2 equivalent molar of CS 6-6-4 in increasing NaCl concentrations.

2.5. Scalar and dipolar coupling constants in glycobiology NMR

Besides chemical shifts, coupling constant values, either scalar (J) or dipolar (D) couplings, both measured in Hz, are another important set of information obtained from

NMR experiment to unveil structural shapes of molecules under certain NMR timescale. In glycobiology, scalar and dipolar couplings are fundamental NMR tools to respectively predict ring conformation, and overall conformational shape of oligosaccharides in solution.

2.5.1. Scalar couplings in conformational analysis of sugar rings

In general, three chemical bond proton-proton ($^3J_{\text{H-H}}$) scalar coupling constants are the most commonly used parameters in 3D conformational shape of sugar rings. This is because that $^3J_{\text{H-H}}$ depends directly upon the dihedral angle of the bonded atoms (Karplus-type relationship). Scalar coupling are usually easily seen by splitting resonances on 1D NMR spectra, but very often, J-resolved NMR experiments must be undertaken for obtaining such values. $^3J_{\text{H-H}}$ can primarily serve as diagnostic for the ring structural conformers of certain glycans. The usefulness of scalar coupling constants can be used by the rule that β -anomers usually exhibit larger $^3J_{\text{H1-H2}}$ values than α - $^1\text{H1}$ -anomers (Table 5, and Figure 2B), which thus help structural assignment. Another example is the GlcNSO_3^- addressed at item 2.2, Figure 6. At normal experimental conditions, N-sulfated glucosamine has its amide group unprotonated as observed by the doublets of doublet of the H2 resonance shown at panel 6B. This is a result from the $^3J_{\text{H-H}}$ coupling of the H2 with H1 and H3. However, at lower temperatures (panel 6C) the H2 resonance showed a splitting resonance of three doublets, meaning $^3J_{\text{H2-H1}}$, $^3J_{\text{H2-H3}}$, and now the protonated NH seen by the third $^3J_{\text{H2-NH}}$. Experimental $^3J_{\text{H-H}}$ values have been determined in many differently sulfated glucosamines, galactosamines and iduronic acids (Tables 5, and 6).

Through the J -values tabulated on Table 5, a sulfation pattern-dependent sugar ring conformation can be clearly noted, except for GalNAc units. And these vicinal coupling constants, for example in α -GlcN,6S is in agreement in various oligo- or polysaccharides containing such monosaccharide [36, 37, 47]. The $^3J_{\text{H1-H2}}$ values ranging from 3.6 to 3.8 Hz for GlcNS; GlcN,6S; GlcN,3,6S; GlcNAc,6S; GalNAc,4S; Glc2,3,4,6S together with the larger coupling values for the other intra-ring protons ($^3J_{\text{H2-H3}}$, $^3J_{\text{H3-H4}}$, $^3J_{\text{H4-H5}}$), somewhere between 8.8 and 11.1 Hz signifies that these monosaccharides are in their $^4\text{C}_1$ chair conformation of the pyranose ring, where the anomeric H1 is in the equatorial position as opposed to the other protons H2, H3, H4, and H5 are in their axial position (Figure 16) [46]. The $^3J_{\text{H-H}}$ values of GalNAc units are also in agreement with the $^4\text{C}_1$ chair conformation regardless the sulfation pattern (4- or 6-sulfated), and the $^3J_{\text{H3-H4}}$ is also compatible with the C4 epimerization of Glc. A different set of $^3J_{\text{H-H}}$ values implying different conformational equilibrium has been determined in hexuronic acids having the non-reducing end 4,5-unsaturation due to an eliminase action (Table 5) [41,43]. These values are consistent with the entire population in the half-chair $^1\text{H}_2$ conformation (Figure 16) in solution [41], and not to the $^2\text{H}_1$ half-chair conformation, which have quite different $^3J_{\text{H-H}}$ values (Table 5).

Residue type	$^3J_{H1-H2}$	$^3J_{H2-H3}$	$^3J_{H3-H4}$	$^3J_{H4-H5}$	Ref.
α -GlcNS	3.6	10.2	9.4	9.9	[36]
α -GlcN,6S	3.6	10.3	9.2	10.0	[37]
α -GlcN,3,6S	3.5	10.7	9.1	10.0	[37]
α -GlcNAc,6S	3.0	11.0	8.0	9.0	[38]
α -GalNAc,4S	3.5	11.0	2.5	nd	[38]
α -GalNAc,6S	4.0	11.0	3.0	nd	[38]
α -Glc2,3,4,6S	3.6	9.8	8.8	nd	[39]
β -Glc2,3,4,6S	5.7	5.2	6.8	6.0	[39]
β -GlcA2,3,4S	6.4	3.2	4.0	2.8	[39]
β -GlcA2,3S	5.9	nd*	1.5	1.5	[40]
α -IdoA (exp) (80:20% 4C_1 : 2S_0)	3.8	8.4	7.6	7.6	[41]
α -IdoA 4C_1 (calc)	2.0	2.1	2.0	2.0	[41]
α -IdoA 2S_0 (calc)	4.3	11.1	5.4	5.4	[41]
α -IdoA (exp) (76:24% 4C_1 : 2S_0)	2.4	4.8	3.4	2.5	[42]
α -IdoA 4C_1 (calc)	1.7	3.0	3.1	2.5	[42]
α -IdoA 2S_0 (calc)	4.8	10.5	3.4	2.5	[42]
Δ HexA (exp)	2.9	1.3	4.8	4.8	[41]
Δ HexA 1H_2 (calc)	3.0	1.5	4.1	4.1	[41]
Δ HexA 2H_1 (calc)	8.3	7.7	2.8	2.8	[41]
Δ HexA (exp) ^a	3.4	2.6	4.7	nd	[42]
Δ HexA (exp+calc) ^b	4.2	2.4	5.0	nd	[42]
Δ HexA 1H_2 (calc)	3.1	0.2	6.0	nd	[42]
Δ HexA 2H_1 (calc)	8.3	10.2	1.7	nd	[42]
Standard 1C_4	1.8	2.6	2.6	1.3	[43]
Standard 2S_0	6.3	9.5	9.3	2.8	[43]
Standard 1H_2	3.2	2.1	4.7	nd	[43]
Standard 2H_1	8.3	7.7	2.8	nd	[43]

^a Experimental values only.

^b Obtained by least square analysis of the theoretical and experimental values combined.

The abbreviations are: exp, experimental values; and calc, calculated values. GlcN, glucosamine; GalN, galactosamine; GlcA, glucuronic acid; IdoA, iduronic acid; Δ hexA, 4,5-unsaturated hexuronic acid; nd, not determined.

Table 5. $^3J_{H-H}$ values (in Hz) in differently sulfated pyranosyl residues from various selected saccharides in solution NMR studies.

Compound number	$^3J_{H1-H2}$	$^3J_{H2-H3}$	$^3J_{H3-H4}$	$^3J_{H4-H5}$	1C_4	4C_1	2S_0	Ref.
1	4.0	6.6	5.2	3.7	45%	29%	26%	[36]
2	1.9	3.7	3.7	2.2	87%	13%	-	[36]
3	1.8	3.3	3.4	2.2	90%	-	10%	[44]
4	4.9	6.9	6.4	4.2	38%	45%	17%	[45]
5	2.5	4.5	2.8	2.2	75%	-	25%	[46]
6	2.5	4.6	3.1	2.3	75%	-	25%	[47]
7	4.0	7.5	3.6	3.1	35%	-	65%	[44]
8	5.2	9.8	4.1	4.0	10%	-	90%	[47]
9	2.6	5.9	3.4	3.1	60%	-	40%	[44]

Table 6. $^3J_{H-H}$ values (in Hz) in composing IdoA units in various selected GAG molecules in solution NMR studies, and the abundance of their 1C_4 , 4C_1 , 2S_0 , 1H_2 , and 2H_1 conformers. These are all experimental values.

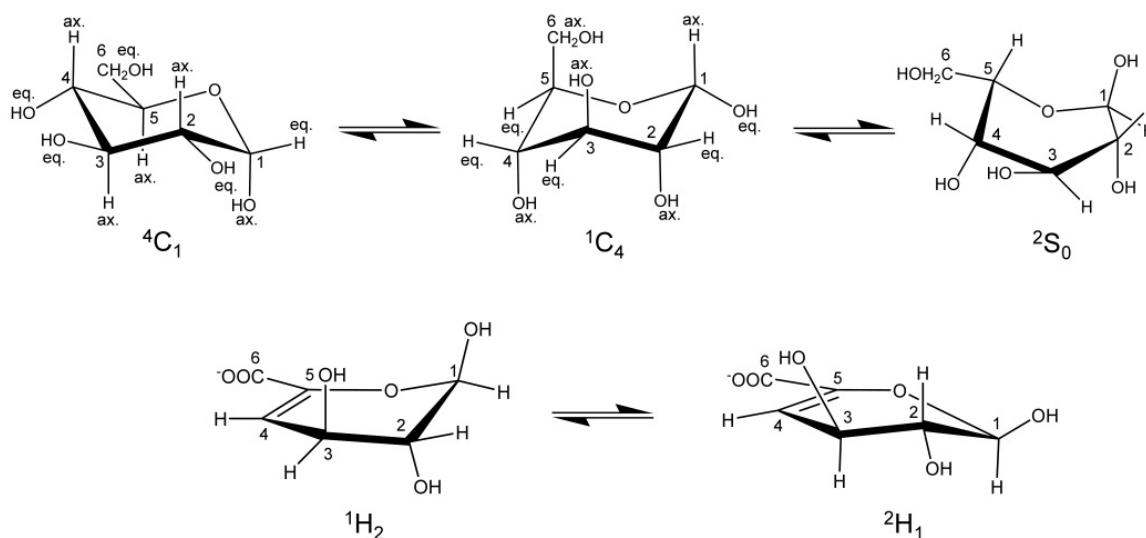


Figure 16. Sugar ring conformations for β -glucopyranosyl units as model for the nomenclatures 4C_1 , 1C_4 , 2S_0 , 1H_2 , and 2H_1 . The latter two conformers have 4,5-unsaturation as a consequence of β -elimination from an eliminase reaction [41, 43]. The carbon numbers are indicated by digits in each conformer.

The conformation set observed for iduronic acid (IdoA) units (Tables 5 and 6), is complex and seems to be influenced not only by their sulfation patterns but also by the adjacent residues in which the IdoA units are linked to. For example, in case of IdoA units of a dermatan sulfate-tetrasaccharide studied at reference [41], the conformer population was estimated through Karplus relationship, and showed the 80/20 ratio for the chair 4C_1 and skew-boat 2S_0 conformations in solution. These IdoA units are linked to GalNAc units in dermatan sulfate, and are not sulfated. But when 2-sulfated or linked to GlcNAc units, as shown in other works presented at Table 6, different population ratios were observed, including the chair 4C_1 conformer together with the chair 1C_4 , and the skew-boat 2S_0 conformers (Figure 16). In a heparin-derived tetrasaccharide, the chair 1C_4 and skew-boat 2S_0 conformer population ratios changed slightly for 76:24% (Table 5) [42]. The half-chair 1H_2 and 2H_1 populations of the unsaturated uronic acid in this heparin-derived tetrasaccharide

changed to the 78:22% ratio [42] rather than 100% ${}^1\text{H}_2$ conformer population for $\Delta 4,5\text{HexA}$ in a dermatan sulfate-derived tetrasaccharide [41] (Table 5) due to the presence of the adjacent GlcNAc unit rather than the GalNAc unit. Therefore, IdoA units can experience different ring conformer population ratios based on the neighboring units (Tables 5 and 6).

2.5.2. Dipolar couplings in conformational studies of oligosaccharides

Dipolar couplings (D) arise from through space spin-spin interactions and are strictly dependent on both inter-nuclear distance (r) and the angle (θ) between the magnetic field (B_0) and the inter-nuclear vector as described by the equation $D_{ij} = \xi_{ij}[(3\cos^2 \theta - 1)/2](1/r^3)$, where ξ_{ij} is a constant that depends on the properties of the nuclei i and j . Dipolar coupling-based NMR data can provide both short-range (distance-dependent) as well as long-range (angular-dependent) structural information [48]. Since the inter-nuclear vector averages to zero in solution through isotropic tumbling, partially aligned molecules, using alignment media such as gels, liquid crystals or polyethylene glycol (PEG), can orient the molecules in solution forcing a partial anisotropic behavior, as the same time the resolution is preserved high in NMR spectra due to some residual fast tumbling in solution [49]. At this condition, the dipolar couplings do not average to zero, and splittings of dipolar coupled spin pairs become measurable [48].

Evidences of spatial structures of oligosaccharides are gradually increasing along the past few years with the advent of specific NMR methods and their application in glycobiology. Although NOE seemed the primary choice in conformational NMR studies, sometimes in the analysis of oligosaccharides the NOE-signal intensity that relies on the efficiency of polarization transfer between proton pairs may go to zero or close to zero because of the correlation time dependence cross-relaxation. In addition, the usual high-order flexibility of oligosaccharides, as opposed to a more rigid structural behavior of nucleic acids and proteins, may result NOE-contacts only from few conformers experienced within a short timescale. This ultimately lowers the efficacy of the NOE-based method in carbohydrate studies. Moreover, while NOE-based structural determination is basically based on through space inter-proton physical contacts, theoretically all types of nuclei pair combinations of spin vectors (${}^1\text{H}$ - ${}^1\text{H}$, ${}^{13}\text{C}$ - ${}^1\text{H}$, ${}^{15}\text{N}$ - ${}^1\text{H}$, ${}^{13}\text{C}$ - ${}^{13}\text{C}$) can be evaluated by the RDC method. Therefore, RDC-based measurements become the alternative NMR method in studies of oligosaccharides, not only on the conformational perspective but also in dynamic analysis. Using residual dipolar couplings (RDC), many carbohydrates have been characterized by the conformational perspective [42, 43, 48]. Here, we briefly revised the conformational and dynamical view of a heparin-tetrasaccharide [$\Delta\text{UA}2\text{SO}_3(1\rightarrow4)\text{-GlcNS,6S-(1}\rightarrow4)\text{-IdoA}2\text{S-(1}\rightarrow4)\text{-GlcNS,6S}$], notated as D-C-B-A, studied by RDC [42]. And in this study, a limited flexibility of the IdoA-composing unit of this tetrasaccharide was unexpectedly observed through the dynamic point-of-view.

Table 7 summarizes experimental ${}^1D_{\text{H-H}}$ and ${}^1D_{\text{H-C}}$ coupling constants of the heparin-derived tetrasaccharide aligned in PEG/hexanol neutral media. The former and the latter couplings were determined from COSY type spectra and ${}^1\text{H}$ -coupled non-refocused ${}^1\text{H}$ - ${}^{13}\text{C}$ HSQC spectra. Five ${}^1D_{\text{C-H}}$ were used to calculate separately the order tensors via singular value

decomposition method [50]. The theoretical RDC values were back calculated using REDCAT [51]. These calculations were performed for both ${}^1\text{C}_4$ and ${}^2\text{S}_0$ conformations of the B ring, the IdoA unit close to the non-reducing end. The comparison between the theoretical and experimental RDCs showed good agreement, proving high accuracy of the measured coupling constants. The better agreement was achieved with the ${}^1\text{C}_4$ conformation of the iduronic acid B unit [42].

Ring	One-bond ${}^1\text{H}$ - ${}^{13}\text{C}$ couplings	J (Hz)	$J + D$ (Hz)	RDC (Hz)	Three-bond ${}^1\text{H}$ - ${}^1\text{H}$ couplings	J (Hz)	$J + D$ (Hz)	RDC (Hz)
A	C1-H1	172.2	168.8	-3.4	H1-H2	3.53	2.71	-0.82
	C2-H2	139.1	144.9	5.8	H2-H3	10.25	11.13	0.88
	C3-H3	148.0	154.1	6.1	H3-H4	8.79	9.75	0.96
	C4-H4	147.2	152.6	5.4	H4-H5	9.85	10.75	0.9
	C5-H5	146.9	153.1	6.2	-	-	-	-
B	C1-H1	174.1	178.9	4.8	H1-H2	2.42	3.97	1.55
	C2-H2	151.4	152.5	1.1	H2-H3	4.76	3.53	-1.22
	C3-H3	151.5	148.9	-2.6	H3-H4	3.41	3.30	-0.11
	C4-H4	148.8	152.8	4.0	-	-	-	-
	C5-H5	146.1	145.7	-0.4	-	-	-	-
C	C1-H1	172.6	177.7	5.1	H1-H2	3.67	2.46	-1.21
	C2-H2	138.7	135.6	-3.1	H2-H3	10.59	11.14	0.55
	C3-H3	147.4	144.4	-3.0	H3-H4	9.04	8.43	-0.61
	C4-H4	147.2	142.4	-4.8	H4-H5	10.16	8.80	-1.36
	C5-H5	147.0	143.4	-3.6	-	-	-	-

Table 7. Scalar and dipolar coupling constants of the heparin-derived tetrasaccharide from the work [41].

In order to obtain the order tensor parameters, the analysis was divided into two sets depending on the conformation of the ring B, and thus, their diagonalized order tensors were inspected. The average Saupe matrix, mostly utilized to build up the molecular frame in RDC-based studies [48], of the ${}^1\text{C}_4$ form was found to have principle axis components: $S_{zz} = 1.44\text{e-}04$, $S_{yy} = 1.36\text{e-}04$, $S_{xx} = -0.70\text{e-}05$ (generalized degree of order, GDO, = $1.62\text{e-}04$), while in the ${}^2\text{S}_0$ form, the values $S_{zz} = 1.58\text{e-}04$, $S_{yy} = 1.43\text{e-}04$, and $S_{xx} = -1.44\text{e-}05$ (GDO = $1.74\text{e-}04$) was given [42]. The GDO is a parameter indicative of molecular motion, and the large difference between GDO of two rigid fragments of a molecule indicates conformational flexibility [42, 48]. The two largest components of the tensors obtained for the heparin-derived tetrasaccharide [42], S_{zz} , and S_{yy} , differ by less than 10%, which caused their occasional swapping, seen in particular for the B ring in the chair ${}^1\text{C}_4$ conformer. Importantly, there is less than 10% difference between the S_{zz} (S_{yy}) values of the two groups of B conformers. In addition, the orientation of the principle axes of the two tensors was very similar. Figure 17 shows that S_{zz} is parallel to the long axis of the trisaccharide CBA of the heparin-derived tetrasaccharide [42]. The large S_{yy} component arises from the presence of bulky sulfate groups, and the fact that the D ring is positioned at an acute angle to the S_{zz} -axis. The smallest component, S_{xx} , is at least an order of magnitude smaller than the others. Although

there is 100% difference between the two forms of ring B, this can easily be a result of small changes in the average orientation of some sulfate groups [42].

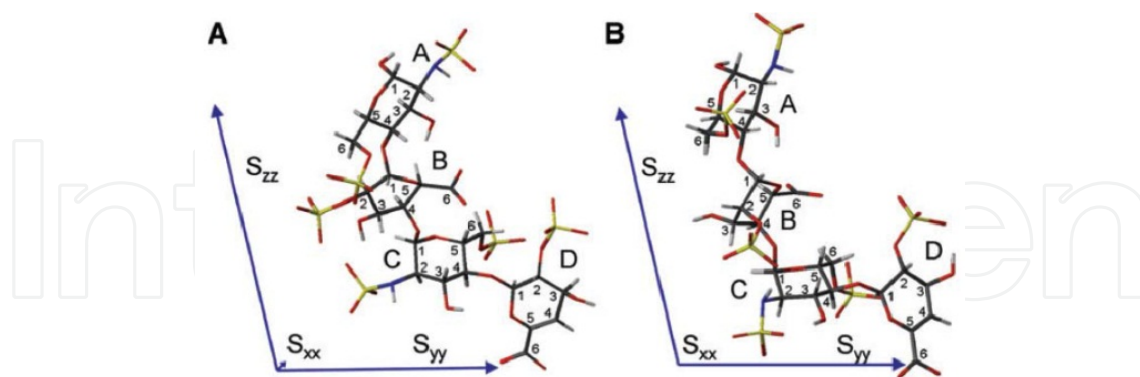


Figure 17. Orientation of the principle axis frame of the order tensor relative to the line-model structure of the heparin-derived tetrasaccharide: (A) ring B in its skew-boat 2S_0 conformation; and (B) ring B in its chair 1C_4 conformation. The relative lengths of the principle axis correspond to the principle order parameters. The rings are indicated by letters and the carbons by digits. White, hydrogen; dark grey, carbon; red, oxygen; blue, nitrogen; yellow, sulfur. Data reproduced from [42].

2.6. NOE in glycobiology NMR

The nuclear Overhauser effect (NOE)-based NMR studies have been considered the foundations of biomolecular NMR not only through the conformational perspective but also useful in deciphering the hydrogen-bond networks of intermolecular complexes containing glycans. This was the main technique applied by the Nobel Prize-awarded group of Kurt Wuthrich in structural studies of biomolecules by NMR spectroscopy. NOE-signals result from a relaxation phenomenon and provide a through-space distance between two nuclei (usually protons) from the same molecule (intra-molecular NOE) from the same residue (intra-residue NOE) or those induced in the presence of binding residue (inter-residue NOE), as well as from different molecules (inter-molecular NOEs). The latter is usually studied by the specific transferred NOE (trNOE)-signals [52]. Next, we will give few brief examples in glycobiology successfully using these two NOE-related NMR techniques.

2.6.1. The classical through space NOE-based structural and conformational studies

As already documented in item 2.5.1, IdoA units can experience in solution the chair 1C_4 , and 4C_1 as well as the skew-boat 2S_0 conformations. The relative proportion of each conformer population varies as function of the adjacent units and attached substituents (if any) [41]. The contribution of each of these conformation populations can be determined by ${}^3J_{H-H}$, but also by intra-residue NOE-signals. In the work of Silipo et al. [41], the NOE contact between H2 and H5 of the IdoA unit, which can only be seen in the skew-boat 2S_0 conformation, supports the ${}^3J_{H-H}$ -based results obtained from a study of a dermatan sulfate-derived tetrasaccharide (Table 5) [41].

Unlikely the previous example of intra-residue NOE-signal, in the work of Castro et al. [53], an intramolecular inter-residue NOE-signal has been assigned between the (1→3) glycosidic

bonds of β -galactosyl units in a marine sulfated galactan. This NOE-signal was crucial to define the repetitive disaccharide unit of this new structure of sulfated glycan [53].

NOE-signals are the most important NMR information for conformational studies, including of carbohydrates. The existence of conformational structures of some oligosaccharides in solution can be seen by the examples of tri-, tetra-, and pentasaccharides of (1 \rightarrow 2)- β -mannopyranosyl units studied by NOESY (nuclear Overhauser effect spectroscopy), and ROESY (rotational frame nuclear Overhauser effect spectroscopy) [54]. These both 2D NMR spectral types are capable to display cross-peaks from through space ^1H - ^1H connections, however, with different intensities as a function of the molecular size or correlation-time. ROE-signals are always positive, ranging from ~40 to 65% intensity, while NOE-signals has larger range, from 50% positive peak intensity to 100% negative peak intensity, according to the molecular size and correlation-time [55]. Therefore, as NOE- and ROE- resonances depend on the size of the molecules, both experiments were recorded for the mannopyranan oligosaccharides [54]. Inter-proton distances were calculated based on the r^{-6} relationship between distance and NOE/ROE cross-peak intensity related to a signal reference from the same studied molecule with known parameters. In this example case, the intra-residue H1-H5 contact, set to 2.39 Å was used found on relevant crystal structure models [54], and the values obtained are displayed in Table 8.

Observed NOE- or ROE-contacts	Inter-proton distances calculated (Å)					
	trisaccharide ^a		tetrasaccharide ^b		pentasaccharide ^a	
Contacts across glycosidic linkage	observed	calculated	observed	calculated	observed	calculated
H2A-H1B	2.3	2.5	2.3	2.4	2.2	2.5
H2B-H1C	2.3	2.4	2.2	2.4	2.2	2.4
H2C-H1D	-	-	2.3	2.5	nq ^c	2.4
H2D-H1E	-	-	-	-	2.3	2.5
Contacts separated by one residue						
H4A-H1C	3.3	2.7	3.1	2.8	3.2	2.9
H4A-H2C	2.9	3.0	2.8	2.7	2.7	2.7
H4B-H1D	-	-	3.1	2.8	3.1	2.9
H4B-H2D	-	-	2.7	3.0	2.7	2.8
H4C-H1E	-	-	-	-	3.2	2.8
H4C-H2E	-	-	-	-	2.8	3.1
Contacts separated by two residues						
H4A-H1D	3.7	3.4	4.1	3.6	3.7	3.4
H4B-H1E	4.2	3.7	-	-	4.2	3.7

^aROE-contacts

^bNOE-contacts

^cnot quantified because of overlap.

Table 8. NOE- or ROE-contacts for (1 \rightarrow 2)- β -mannopyranosyl units tri-, tetra- and pentasaccharides. Oligosaccharides are labeled from the reducing terminus. Reproduced from [54].

All the inter-glycosidic contacts (H1-H2) between linked mannosyl units are assigned and with similar distance values (Table 8). The rising numbers of other spatial contacts in tri-, tetra- and pentasaccharide, point clearly towards defined 3D conformers of these molecules. The presence of contacts between H4 with H1 and H2 of residues located two units away in a chain, strikingly supports the presence of ordered structures of these oligosaccharides in solution [54].

2.6.2. Protein-bound carbohydrate conformations seen by transferred NOE

Transferred NOE (trNOE) experiments can reveal the bioactive conformations of protein-bound carbohydrates [56-59]. This is very important in glycobiology since the recognition of binding conformers of sugars to enzymes, antibodies and lectins are of great interest in glycobiology, especially for in carbohydrate-based drug design. trNOE is obtained from a regular NOESY experiment although at a protein-carbohydrate mixed samples that possess some dynamic exchange. The carbohydrate ligand must be in excess of the protein, and thus trNOE can be collected from the free ligand that experience the "on-state" upon physical contact with the protein. In complexes involving large molecules, cross-relaxation rates of the bound state (σ^B), which depend on the respective inter-proton distances, the spectrometer frequency, and the correlation time (molecular size) of the complex, have opposite sign compared to the free state (σ^F), and produce negative resonance. Therefore, the existence of binding formation can be proved by simple visual inspection since the small molecules, free ligands, would produce positive NOE signals. For a trNOE experiment, the following conditions must occur: 1) $\text{PROTEIN} + \text{SUGAR}_{(\text{excess})} \leftrightarrow \text{PROTEIN.SUGAR}$, 2) $K_a = [\text{PROTEIN.SUGAR}] / [\text{PROTEIN}] \times [\text{SUGAR}]$, 3) $p_b \sigma^B > p_f \sigma^F$, and 4) $k_{-1} \gg \sigma^B$, where K_a is the association constant, p_b and p_f are the fractions of bound and free sugar ligand, σ^B and σ^F are the cross-relaxation rates for the bound and unbound ligand states, and k_{-1} is the off-rate constant. Therefore, based on the fourth rule, the exchange reaction has to be fast on the relaxation timescale.

The use of trNOE can be illustrated by the work concerning the protein-bound conformational characterization of the mimetic ligand β -D-GlcpNAc-(1 \rightarrow 2)- α -D-Manp-(1 \rightarrow 6)- β -D-Glcp-O-Octyl, an acceptor of the enzyme N-acetylglucosaminyltransferase V (GnT-V) [59]. Figure 18 shows an expansion of the glycosyl region at NOESY spectra of the carbohydrate acceptor substrate, in the presence of the enzyme, and the enzyme only. Regardless the cross-peaks from the protein (Figure 18c), Figure 18b showed a number of cross-peaks not observed in the free acceptor (Figure 18a). These are trNOE that were used as distance constraints (Table 9) for modeling a GnT-V-bound conformation of the ligand (Figure 19). Simulated annealing was used to refine the structure of the bound-state acceptor using the NOE constraints listed in Table 9. From the 100 structures generated, an ensemble of the selected 10 lowest overall energy conformations-built structure is illustrated in Figure 19. With this example, trNOE-based NMR studies are shown to be quite efficient to determine, protein-bound conformational states of carbohydrates.

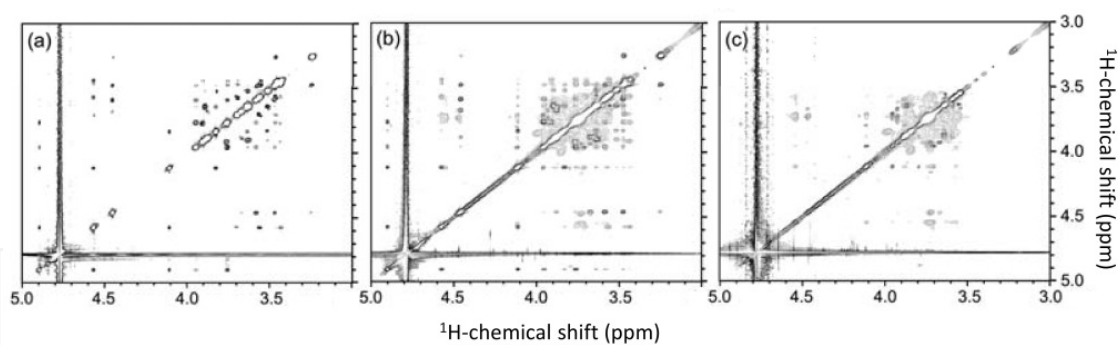


Figure 18. Expanded (carbohydrate region) NOESY spectra of (a) the acceptor, (b) the acceptor in the presence of GnT-V, and (c) GnT-V background. These allow assessment of conformational changes on binding to GnT-V. Reproduced from [59].

O-Octyl	Glc	Man'	GlcNAc''	Distances (Å)
CH2-1b	H1	-	-	3.0
CH2-1a	H1	-	-	3.0
CH2-2	H1	-	-	3.5
-	H5-H6(S)	-	-	2.2
-	H1-H6(S)	-	-	3.3
-	H6(S)	H1'	-	2.5
-	H6(S)	H2'	-	2.9
-	H4	H3'	-	3.0
-	H5	H1'	-	3.5
-	H4	H1'	-	3.9
-	H6(S)	-	H1''	3.0
-	H6(S)	-	NAc	3.6
-	-	H4-H6(S)	-	2.9
-	-	H2'	H1''	2.6
-	-	H1'	H1''	2.7
-	-	H2'	H5''	3.5
-	-	H1'	NAc	3.5
-	-	H3'	H1''	3.6
-	-	H6'(S)	NAc	3.6
-	-	H2'	H4''	3.7
-	-	H1'	H5''	4.1
-	-	H2'	NAc	4.8
-	-	H4'	NAc	4.9
-	-	-	H5''-H6''(R)	2.5
-	-	-	H5''-H6''(S)	2.5
-	-	-	H4''-H6''(S)	3.1
-	-	-	H1''-NAc	4.0
-	-	-	H2''-NAc	4.5
-	-	-	H3''-NAc	

Table 9. ^1H - ^1H distances determined from the trNOE signals from the acceptor in the presence of GnT-V. Data reproduced from [59].

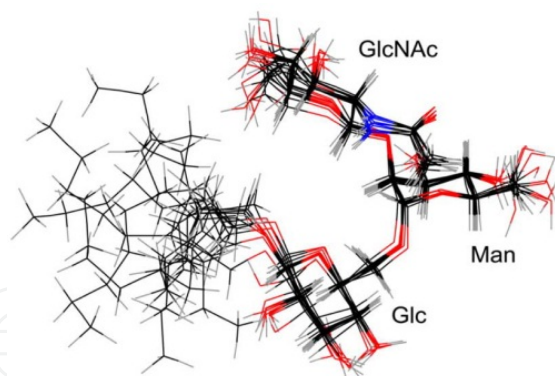


Figure 19. The 10 lowest energy structures from NOE restrained simulated annealing were aligned using the sugar ring atoms. Note the higher disorder at the O-octyl chain. Reproduced from [59].

3. Marked conclusions

Despite the recent association of NMR with glycobiology, relevant results have ultimately appeared. Although carbohydrates possess high-order degrees of flexibility, and usually great structural complexity; NMR methods still seem quite able to elucidate the main structural characteristics and dynamic behaviors of the majority of glycans. Since NMR spectroscopy is currently the most advanced and powerful structural technique, despite its sensitivity issue, its contribution to the glycobiology's progress, and thus to the current glycomics' is profound. New NMR methods have been adjusted just for carbohydrate analysis, inclusively specific isotopic labeling protocols to overcome the sensitivity problem. Proton, carbon-13, nitrogen-15 by either one- or multi-dimensional NMR experiments, chemical shifts, scalar coupling constants, dipolar coupling constants, and NOE-through space connections of free or protein-bound carbohydrates comprise the principle NMR spectroscopy methods for glycobiology. Many other NMR techniques, such as saturation transfer difference and modified pulse sequence destined just to address glycobiology-related problems do exist, although not covered in this chapter. The main idea of carbohydrates as just energetically or structurally involved-molecules, has falling apart as many other vital functions of glycans, mostly in signaling events, have been unraveled along the past few years. And NMR spectroscopy is making an outstanding contribution for these big discoveries.

Author details

Vitor H. Pomin

Program of Glycobiology, Institute of Medical Biochemistry, University Hospital Clementino Fraga Filho, Federal University of Rio de Janeiro, Rio de Janeiro, Brazil

Acknowledgement

The author acknowledges InTech-Open Access Publisher for the kind invitation in contributing with this chapter; Dr. John Glushka to the help on the GlcNS assignment; Dr.

Ana Paula Valente to the help on the ^{13}C -direct observe spectrum of Glc, and the accessibility to the Bruker 400 MHz spectrometer; and Prof. James H. Prestegard for all NMR background during my post-doctorate period, and the accessibility at the Varian 800 MHz spectrometer. All the data discussed in this chapter in which the Varian 800 MHz is indicated in figure legends, were recorded during the author's post-doctorate period at Complex Carbohydrate Research Center, the University of Georgia, US under the partial financial support from the National Center for Research Resources of the National Institute of Health, RR005351, and from the post-doctoral fellowship (PDE #201019/2008-6) from Conselho Nacional de Desenvolvimento Científico e Tecnológico (CNPq), Brazil.

4. References

- [1] Kurt Wüthrich (1986) *NMR of Proteins and Nucleic Acids*, Wiley Interscience, pg 1.
- [2] LeMaster DM, Richards FM (1982) Preparative-scale isolation of isotopically labeled amino acids. *Anal. biochem.* 122: 238-247.
- [3] Kainosho M, Tsuji T (1982) Assignment of the three methionyl carbonyl carbon resonances in *Streptomyces subtilisin* inhibitor by a carbon-13 and nitrogen-15 double-labeling technique. A new strategy for structural studies of proteins in solution. *Biochem.* 21: 6273-6279.
- [4] Pervushin K, Riek R, Wider G, Wüthrich K (1997) Attenuated T2 relaxation by mutual cancellation of dipole-dipole coupling and chemical shift anisotropy indicates an avenue to NMR structures of very large biological macromolecules in solution. *Proc. natl. acad. sci. USA.* 94: 12366-12377.
- [5] Salzmann M, Pervushin K, Wider G, Senn H, Wüthrich K (1998) TROSY in triple-resonance experiments: new perspectives for sequential NMR assignment of large proteins. *Proc. natl. acad. sci. USA.* 95: 13585-13590.
- [6] Liu Y, Prestegard JH (2011) Multi-dimensional NMR without coherence transfer: minimizing losses in large systems. *J. magn. reson.* 212: 289-298.
- [7] Pervushin K, Ono A, Fernández C, Szyperski T, Kainosho M, Wüthrich K (1998) NMR scalar couplings across Watson-Crick base pair hydrogen bonds in DNA observed by transverse relaxation-optimized spectroscopy. *Proc. natl. acad. sci. USA.* 95: 14147-14151.
- [8] Riek R, Wider G, Pervushin K, Wüthrich K (1999) Polarization transfer by cross-correlated relaxation in solution NMR with very large molecules. *Proc. natl. acad. sci. USA.* 96: 4918-4923.
- [9] Fiala R, Czernek J, Sklenář V (2000) Transverse relaxation optimized triple-resonance NMR experiments for nucleic acids. *J. biomol. NMR.* 16: 291-302.
- [10] Pomin VH, Sharp JS, Li X, Wang L, Prestegard JH (2010) Characterization of glycosaminoglycans by ^{15}N NMR spectroscopy and in vivo isotopic labeling. *Anal. chem.* 82: 4078-4088.
- [11] Parella T, Nolis P (2005) Spin-edited 2D HSQC-TOCSY experiments for the measurement of homonuclear and heteronuclear coupling constants: application to carbohydrates and peptides. *J. magn. reson.* 176: 15-26.

- [12] Zhang Q, Li N, Liu X, Zhao Z, Li Z, Xu Z (2004) The structure of a sulfated galactan from *Porphyra haitanensis* and its *in vivo* antioxidant activity. *Carbohydr. res.* 339: 105-111.
- [13] Kolender AA, Matulewicz MC (2002) Sulfated polysaccharides from the red seaweed *Georgiella confluens*. *Carbohydr. res.* 337: 57-68.
- [14] Liao ML, Chiovitti A, Munro SL, Craik DJ, Kraft GT, Bacic A (1996) Sulfated galactans from Australian specimens of the red alga *Phacelocarpus peperocarpus* (Gigartinales, Rhodophyta). *Carbohydr. res.* 296: 237-247.
- [15] Langeslay DJ, Beni S, Larive CK (2011) Detection of the ^1H and ^{15}N NMR resonances of sulfamate groups on aqueous solution: a new tool for heparin and heparan sulfate characterization. *Anal. chem.* 83: 8006-8010.
- [16] Gomes AM, Kozłowski EO, Pomin VH, de Barros CM, Zaganeli JL, Pavão MS (2010) Unique extracellular matrix heparan sulfate from the bivalve *Nodipecten nodosus* (Linnaeus, 1758) safely inhibits arterial thrombosis after photochemically induced endothelial lesion. *J. biol. chem.* 285: 7312-7323.
- [17] Jiménez-Barbero J, Peters J (2003) *NMR spectroscopy of glycoconjugates*, Wiley-VCH, pg 4.
- [18] Barb AW, Prestegard JH (2011) NMR analysis demonstrates immunoglobulin G N-glycans are accessible and dynamics. *Nat. chem. biol.* 7: 147-153.
- [19] Scalan CN, Burton DR, Dwek RA (2008) Making antibodies safe. *Proc. natl. acad. sci. USA.* 105: 4081-4082.
- [20] Kaneko Y, Nimmerjahn F, Ravetch JV (2006) Anti-Inflammatory Activity of Immunoglobulin G Resulting from Fc Sialylation. *Science.* 313: 670-673.
- [21] Tsuchiya N, Endo T, Matsuta K, Yoshinoya S, Aikawa T, Kosuge E, Takeuchi F, Miyamoto T, Kobata A (1989) Effects of galactose depletion from oligosaccharide chains on immunological activities of human IgG. *J. rheumatol.* 16: 285-290.
- [22] Nimmerjahn F, Anthony RM, Ravetch JV (2007) Agalactosylated IgG antibodies depend on cellular Fc receptors for *in vivo* activity. *Proc. natl. acad. sci. USA.* 104: 8433-8437.
- [23] Malhotra R, Wormald MR, Rudd PM, Fischer PB, Dwek RA, Sim RB (1995) Glycosylation changes of IgG associated with rheumatoid arthritis can activate complement via the mannose-binding protein. *Nat. med.* 1: 237-243.
- [24] Shields RL, Lai J, Keck R, O'Connell LY, Hong K, Meng YG, Weikert SH, Presta LG (2002) Lack of fucose on human IgG1 N-linked oligosaccharide improves binding to human Fc γ RIII and antibody-dependent cellular toxicity. *J. biol. chem.* 277: 26733-26740.
- [25] Teng Q (2005) *Structural biology – Practical NMR applications*. Springer Science, pg 253-258.
- [26] Cavanagh J (2007) *Protein NMR Spectroscopy: Principles and Practice*. 2nd ed., Academic Press, pg 711.
- [27] Kurt Wüthrich (1986) *NMR of Proteins and Nucleic Acids*, Wiley Interscience, pg 1.
- [28] Teng Q (2005) *Structural biology – Practical NMR applications*. Springer Science, pg 18.
- [29] Teng Q (2005) *Structural biology – Practical NMR applications*. Springer Science, pg 3-4.

- [30] Martin L, Blanpain C, Garnier P, Wittamer V, Parmentier M, Vita C (2001) Structural and Functional Analysis of the RANTES-Glycosaminoglycans Interactions. *Biochem.* 40: 6303-6318.
- [31] Hoogewerf AJ, Kuschert GS, Proudfoot AE, Borlat F, Clark-Lewis J, Power CA, Wells TN (1997) Glycosaminoglycans mediate cell surface oligomerization of chemokines. *Biochem.* 36: 13570-13578.
- [32] Wang X, Watson C, Sharp JS, Handel TM, Prestegard JH. (2011) Oligomeric structure of the chemokine CCL5/RANTES from NMR, MS, and SAXS data. *Structure.* 19: 1138-1148.
- [33] Proudfoot AE, Fritchley S, Borlat F, Shaw JP, Vilbois F, Zwahlen C, Trkola A, Marchant D, Clapham PR, Wells TN. (2001) The BBXB motif of RANTES is the principal site for heparin binding and controls receptor selectivity. *J. biol. chem.* 276: 10620-10626.
- [34] Pomin VH, Park Y, Huang R, Heiss C, Sharp JS, Azadi P, Prestegard JH (2012) Exploiting enzyme specificities in digestions of chondroitin sulfates A and C: production of well-defined hexasaccharides. *Glycobiology*, 22: 826-838.
- [35] Czaplewski LG, McKeating J, Craven CJ, Higgins LD, Appay V, Brown A, Dudgeon T, Howard LA, Meyers T, Owen J, Palan SR, Tan P, Wilson G, Woods NR, Heyworth CM, Lord BI, Brotherton D, Christison R, Craig S, Cribbes S, Edwards RM, Evans SJ, Gilbert R, Morgan P, Randle E, Schofield N, Varley PG, Fisher J, Waltho JP, Hunter MG (1999) Identification of amino acid residues critical for aggregation of human CC chemokines macrophage inflammatory protein (MIP)-1 alpha, MIP-1 beta, and RANTES - Characterization of active disaggregated chemokine variants. *J. biol. chem.* 274: 16077-16084.
- [36] van Boeckel CAA, van Aelst SF, Wagenaars GN, Mellema J-R, Paulsen H, Peters T, Pollex A, Sinnwell V (1987) Conformational analysis of synthetic heparin-like oligosaccharides containing α -L-idopyranosyluronic acid. *Recl. trav. chim. pays-bas.* 106: 19-29.
- [37] Torri G, Casu B, Gatti G, Petitou M, Choay J, Jacquinet JC, Sinaÿ P (1985) Mono- and bidimensional 500 MHz ¹H-NMR spectra of a synthetic pentasaccharide corresponding to the binding sequence of heparin to antithrombin-III: evidence for conformational peculiarity of the sulfated iduronate residue. *Biochem. biophys. res. com.* 128: 134-140.
- [38] Yamada S, Yoshida K, Sugiura M, Sugahara K (1992) One- and two-dimensional ¹H-NMR characterization of two series of sulfated disaccharides prepared from chondroitin sulfate and heparan sulfate/heparin by bacterial eliminase digestion. *J. biochem.* 112: 440-447.
- [39] Wessel HP, Bartsch S (1995) Conformational flexibility in highly sulfated beta-D-glucopyranoside derivatives. *Carbohydr. res.* 274: 1-9.
- [40] Maruyama T, Toida T, Imanari T, Yu G, Linhardt RJ.(1998) Conformational changes and anticoagulant activity of chondroitin sulfate following its O-sulfonation. *Carbohydr. res.* 306: 35-43.
- [41] Silipo A, Zhang Z, Cañada FJ, Molinaro A, Linhardt RJ, Jiménez-Barbero J (2008) Conformational analysis of a dermatan sulfate-derived tetrasaccharide by NMR, molecular modeling, and residual dipolar coupling. *ChemBiochem.* 9: 240-252.

- [42] Jin L, Hricovíni M, Deakin JA, Lyon M, Uhrín D (2009) Residual dipolar coupling investigation of a heparin tetrasaccharide confirms the limited effect of flexibility of the iduronic acid on the molecular shape of heparin. *Glycobiology*. 19: 1185-1196.
- [43] Mikhalov D, Linhardt RJ, Mayo KH (1997) NMR solution conformation of heparin-derived hexaccharide. *Biochem. j.* 328: 51-61.
- [44] Ferro DR, Provasoli A, Ragazzi M, Torri G, Casu B, Gatti G, Jacquinet JC, Sinay P, Petitou M, Choay J (1986) Evidence for conformational equilibrium of the sulfated L-iduronate residue in heparin and in synthetic heparin mono- and oligo-saccharides: NMR and force-field studies. *J. am. chem. soc.* 108: 6773-6778.
- [45] Foster MJ, Mulloy B (1993) Molecular dynamics study of iduronate ring conformation. *Biopolymers*. 33: 575-588.
- [46] Hricovíni M, Guerrini M, Bisio A (1999) Structure of heparin-derived tetrasaccharide complexed to the plasma protein antithrombin derived from NOEs, J-couplings and chemical shifts. *Eur. j. biochem.* 261: 789-801.
- [47] Jiménez-Barbero J, and Peters T (2003) *NMR Spectroscopy of Glycoconjugates*, Wiley-VCH, pg 197.
- [48] Tian F, Al-Hashimi HM, Craighead JL, Prestegard JH (2001) Conformational analysis of a flexible oligosaccharide using residual dipolar couplings. *J. am. chem. soc.* 123: 485-492.
- [49] Prestegard JH, Al-Hashimi HM, Tolman JR (2000) NMR structures of biomolecules using field oriented media and residual dipolar couplings. *Q. rev. biophys.* 33: 371-424.
- [50] Losonczi JA, Andrec M, Fischer MW, Prestegard JH (1999) Order matrix analysis of residual dipolar couplings using singular value decomposition. *J. magn. reson.* 138: 334-342.
- [51] Valafar H, Prestegard JH (2004) REDCAT: a residual dipolar coupling analysis tool. *J. magn. reson.* 167: 228-241.
- [52] Willianson MP (2006) The transferred NOE. *Modern magn. reson.* 28: 1357-1362.
- [53] Castro MO, Pomin VH, Santos LL, Vilela-Silva AC, Hirohashi N, Pol-Fachin L, Verli H, Mourão PA (2009) A unique 2-sulfated {beta}-galactan from the egg jelly of the sea urchin *Glyptocidaris crenularis*: conformation flexibility versus induction of the sperm acrosome reaction. *J. biol. chem.* 284: 18790-18800.
- [54] Jiménez-Barbero J, and Peters T (2003) *NMR Spectroscopy of Glycoconjugates*, Wiley-VCH, pg 160-168.
- [55] Otter A, Kotovych (1988) The solution conformation of the synthetic tubulin fragment Ac-tubulin- α (430-441)-amide based on two-dimensional ROESY experiments. *Can. j. chem.* 66: 1814-1820.
- [56] Angulo J, Rademacher C, Biet T, Benie AJ, Blume A, Peters H, Palcic M, Parra F, Peters T (2006) NMR analysis of carbohydrate-protein interactions. *Methods enzymol.* 416: 12-30.
- [57] Bevilacqua VL, Thomson DS, Prestegard JH (1990) Conformation of methyl beta-lactoside bound to the ricin B-chain: interpretation of transferred nuclear Overhauser effects facilitated by spin simulation and selective deuteration. *Biochem.* 29: 5529-5537.

- [58] Bevilacqua VL, Kim Y, Prestegard JH (1992) Conformation of beta-methylmelibiose bound to the ricin B-chain as determined from transferred nuclear Overhauser effects. *Biochem.* 31: 9339-9349.
- [59] Macnaughtan MA, Kamar M, Alvarez-Manilla G, Venot A, Glushka J, Pierce JM, Prestegard JH (2007) NMR structural characterization of substrates bound to N-acetylglucosaminyltransferase V. *J. mol. biol.* 366: 1266-1281.

IntechOpen

IntechOpen